S-wave contribution to rare $D^0 \to \pi^+\pi^-\ell^+\ell^-$ decays in the standard model and sensitivity to new physics

Svjetlana Fajfer,[1] Eleftheria Solomonidi,[2] and Luiz Vale Silva[2]

[1]*Jožef Stefan Institute, Jamova 39, P. O. Box 3000, 1001 Ljubljana, Slovenia and Faculty of Mathematics and Physics, University of Ljubljana, Jadranska 19, 1000 Ljubljana, Slovenia*

[2]*Departament de Física Teòrica, Instituto de Física Corpuscular, Universitat de València—Consejo Superior de Investigaciones Científicas, Parc Científic, Catedrático José Beltrán 2, E-46980 Paterna, Valencia, Spain*

(Received 17 December 2023; accepted 24 January 2024; published 26 February 2024)

Physics of the up-type flavor offers unique possibilities of testing the standard model (SM) compared to the down-type flavor sector. Here, we discuss SM and new physics (NP) contributions to the rare charm-meson decay $D^0 \to \pi^+\pi^-\ell^+\ell^-$. In particular, we discuss the effect of including the lightest scalar isoscalar resonance in the SM picture, namely, the $f_0(500)$, which manifests in a big portion of the allowed phase space. Other than showing in the total branching ratio at an observable level of about 20%, the $f_0(500)$ resonance manifests as interference terms with the vector resonances, such as at high invariant mass of the leptonic pair in distinct angular observables. Recent data from LHCb optimize the sensitivity to P-wave contributions that we analyze in view of the inclusion of vector resonances. We propose the measurement of alternative observables that are sensitive to the S-wave and are straightforward to implement experimentally. This leads to a new set of null observables that vanish in the SM due to its gauge and flavor structures. Finally, we study observables that depend on the SM interference with generic NP contributions from semileptonic four-fermion operators in the presence of the S-wave.

DOI: 10.1103/PhysRevD.109.036027

I. INTRODUCTION

Rare decays played a crucial role in building the standard model (SM): it is, for instance, thanks to $K_L \to \mu^+\mu^-$ that one gathered indirect information about the existence of the charm quark before its discovery [1]. Rare charm-meson decays provide complementary information to down-type flavor changing neutral currents (FCNCs) transitions. However, given the effectiveness of the Glashow-Iliopoulos-Maiani (GIM) suppression in up-type FCNCs, and the almost diagonal structure of the Cabibbo-Kobayashi-Maskawa (CKM) matrix, this class of transitions is very sensitive to the strong dynamics: as we will see, the available phase space in charm-meson decays is entirely populated with "intermediate" resonance peaks and their tails, in contrast to analogous bottom-meson decays. Therefore, for the sake of new physics (NP) searches in rare charm-meson decays, the SM has to be described sufficiently well; this is so when the SM acts as a background, and it is also the case when one wants to understand the SM-NP interference in order to set bounds on the NP properties.

LHCb will largely improve measurements of rare D meson decay channels; for very recent experimental analyses of $D^0 \to \pi^+\pi^-\mu^+\mu^-$ and $D^0 \to K^+K^-\mu^+\mu^-$, see the analysis of Refs. [2–4] that extends Refs. [5–8]. The total branching fractions are [6]

$$\begin{aligned}\mathcal{B}(D^0 \to \pi^+\pi^-\mu^+\mu^-) &= (9.6 \pm 1.2) \times 10^{-7},\\ \mathcal{B}(D^0 \to K^+K^-\mu^+\mu^-) &= (1.5 \pm 0.3) \times 10^{-7}.\end{aligned} \quad (1)$$

Limits on the electronic mode $D^0 \to \pi^+\pi^-e^+e^-$ branching ratio are discussed in Refs. [9,10], with good prospects of improvement at the Super Tau-Charm Facility [11]. A rich angular analysis is possible, resulting from the high multiplicity of the final state. This promising experimental program has to be matched by an increased theoretical precision. Our ultimate goal here is to provide more robust tests of NP contributions possibly affecting these rare charm-meson decays. For this reason, we reassess the description of the SM contributions. As it will be discussed in this article, present data already allow for an enhanced control over the SM background, i.e., contributions of intermediate resonances, and their relative strong phases.

As a result, we will then in particular be able to point out improved observables for NP searches.

We focus here on the inclusion of intermediate resonances in the description of the decay $D^0 \to \pi^+\pi^-\ell^+\ell^-$ (ℓ are electrons or muons); we reserve the mode $D^0 \to K^+K^-\ell^+\ell^-$ for future work.[1] The strategy adopted is to consider quasi-two-body decays, where the pion pair in the final state originates from strong decays of resonances such as the $\rho(770)^0 \equiv \rho^0$, while the lepton pair originates from electromagnetic (EM) decays of states such as η, $\eta'(958) \equiv \eta'$, ρ^0, $\omega(782) \equiv \omega$, and $\phi(1020) \equiv \phi$. The vector resonances are clearly seen in the data collected by LHCb [2–4]. For previous theoretical analyses, see, for instance, Refs. [12–17]; also, see Refs. [18,19] in the framework of QCD factorization at low-$q^2(\ell^+\ell^-)$ (while as it will be later discussed we avoid this region), where the hadronic uncertainties in this framework are quantitatively assessed, and also for the use of an operator product expansion (OPE) in the very high-$q^2(\ell^+\ell^-)$ region (which for different reasons we also avoid, as discussed later). Other cases of interest in assessing SM contributions in related rare (semi)leptonic charm-meson decay modes include the ones of Refs. [19–23] (while Ref. [24] discusses the mode $D_s^+ \to \pi^+\ell^+\ell^-$, not mediated by FCNCs). See also Ref. [25] for a recent theoretical and experimental review.

Beyond the vector and pseudoscalar resonances aforementioned, further resonances could also lead to an important SM contribution. We have identified the scalar isoscalar state $f_0(500) \equiv \sigma$ as a relevant contribution not previously included in past analyses (although pointed out in Ref. [17]). Such a broad state leaves its footprints in the rescattering of pion pairs [26,27]; note that the PDG [28] minireview on scalar mesons below 1 GeV quotes for the σ pole position the value $(449^{+22}_{-16}) - i(275 \pm 12)$ MeV stemming from "the most advanced dispersive analyses," which is a precision better than 5%. As it will be discussed in this article, although the S-wave does not affect some angular observables (in particular, those based in I_i, $i = 3$, 6, 9 [17]), it affects a large set of them (i.e., some observables built from I_i, $i = 1$, 2, 4, 5, 7, 8), and thus provides novel null tests of the SM when the NP interferes with the SM in the presence of the S-wave.

We highlight that the S-wave contribution has already been observed in semileptonic charm-meson decays. BESIII [29] has seen an S-wave contribution coming from σ at the level of 26% of the total branching ratio of $D^+ \to \pi^+\pi^-e^+\nu_e$. It is worth stressing that this occurs in the absence of interference with the dominant P-wave, as is the case for the total branching ratio; also note that this contribution does not manifest as a distinguished peak in the invariant mass of the final pion pair. Instead, the S-wave effect can be better spotted from its interference with the dominant P-wave contribution (mainly coming from $\rho^0 \to \pi^+\pi^-$) in alternative observables: a pronounced asymmetry is thus clearly seen in the differential branching ratio as a function of the angle θ_π describing the orientation of the pion pair. Accordingly, no pronounced asymmetry is seen in $D^0 \to \pi^-\pi^0e^+\nu_e$, for which the S-wave contribution is absent. One could expect even more explicit manifestations of the S-wave in the differential branching ratio as a function of θ_π and the angle ϕ between the decay planes of the lepton and pion pairs, when integrating over carefully chosen slices of the invariant mass of the pion pair, as seen, for instance, in the analogous analysis of the Cabibbo, allowed mode $D^+ \to K^-\pi^+e^+\nu_e$ by *BABAR* [30], where the S-wave contribution, in particular, from $K_0^*(800) \equiv \kappa$ and $K_0^*(1430)$, is at the level of 6%; see also Refs. [31,32]. This shows that some angular observables can be directly used to investigate the P- and S-wave interference.

Moreover, although uncertainties are still large, an amplitude analysis of CLEO data [33] of $D^0 \to \pi^+\pi^-\pi^+\pi^-$ indicates an important contribution of $D^0 \to \sigma\rho^0$, comparable to the contributions of $D^0 \to \rho^0\rho^0$. The very recent analysis by BESIII [34] distinguishes more clearly a contribution from the former. Other topologies affecting rare decays are suggested by the amplitude analyses of multihadronic decays $D^0 \to \pi^+\pi^-\pi^+\pi^-$ and $D^0 \to K^+K^-\pi^+\pi^-$ [33,35], namely, so-called cascade decays in which there is an intermediate $a_1(1260)^\pm$ (which affects $D^0 \to \pi^+\pi^-\ell^+\ell^-$) or $K_1(1270)^\pm$ (which affects $D^0 \to K^+K^-\ell^+\ell^-$). Such states would not manifest as peaks in the invariant mass of the lepton or light hadron pairs, since they involve a distinct combination of kinematical variables. In these topologies, the lepton pair results from ρ^0 and ϕ, while the pion and kaon pairs are nonresonant. Given that the axial vector resonances above are known to a lesser extent than those resonances included in our analysis, we reserve their analysis for future work.

Our study provides the first analysis of the S-wave in rare charm-meson decays, and we discuss what can be learnt from this physics case; we focus on the σ resonance, which alone impacts a large portion of the allowed phase space; see Fig. 1 (that extends a figure from Ref. [17]). Considering other scalar isoscalar resonances, let us point out the following: $f_0(980)$ is included in the analysis of Ref. [29], and is not observed to provide a significant contribution; $f_0(1370)$ is a very broad resonance that "overlaps" partially with $\rho^0/\omega \to \ell^+\ell^-$ in the $q^2(\ell^+\ell^-)$ vs $p^2(\pi^+\pi^-)$ plane; $f_0(1500)$ (of width ~100 MeV [28])

[1]The lightest resonances coupling more strongly to the kaon pair are $f_0(980)$ and $\phi(1020)$, which manifest at similar energies, the latter being very narrow though; this may produce an interesting interference pattern between the S- and P-waves in angular observables. A representation of the line shape of the scalar isoscalar resonance is more difficult to achieve due to its proximity to the kaon pair threshold.

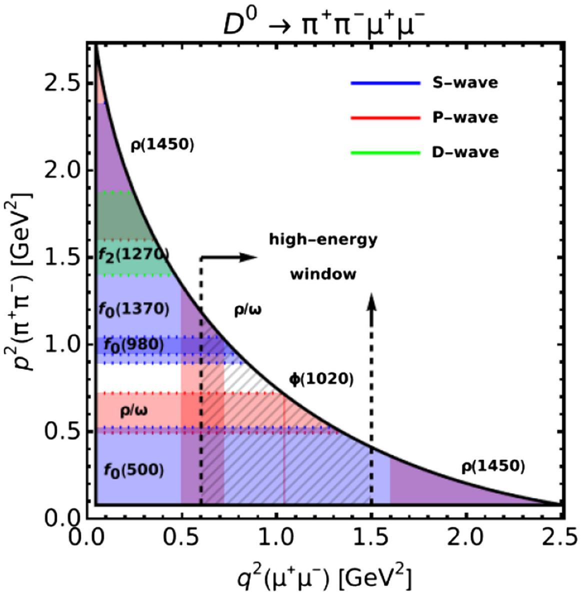

FIG. 1. Phase space allowed in the decay $D^0 \to \pi^+\pi^-\mu^+\mu^-$; the invariant mass of the pion (muon) pair is denoted p^2 (respectively, q^2). Some scalar (blue), vectorial (red), and tensorial (green) resonant contributions are shown (the very narrow pseudoscalar resonances $\eta^{(\prime)}$, leading to the lepton pair via two-photon exchange, are omitted); the bands correspond to $(m \pm \Gamma/2)^2$, with Γ taken from Refs. [27,28,38,39]. The "high-energy window" referred to in the plot corresponds to $m^2_{\rho^0} \lesssim q^2 \lesssim 1.5$ GeV^2, for which only $f_0(500) \equiv \sigma$ gives an important contribution among the S-wave contributions and is indicated by a hashed pattern delimited by dashed vertical lines. Cascade decays are not indicated.

has an important branching ratio into pion pairs of approximately 35% [28], but is restricted to a region that "overlaps" little with $\rho^0/\omega \to \ell^+\ell^-$; similarly, $f_0(1710)$ (of width ~100 MeV [28]) is also restricted to the low-energy window of the lepton pair. On the other hand, more is known about the lightest S- and P-wave states, which affect a more significant portion of the phase space. Therefore, we will not include S-wave resonances other than the σ. Instead, we focus on energies $q^2(\ell^+\ell^-) \gtrsim m^2_{\rho^0}$, reducing the need to include further contributions. Given the kinematical window we focus on, we do not discuss the bremsstrahlung contribution (where a soft photon is emitted from $D^0 \to \pi^+\pi^-$); see Refs. [16,36] for its description, which is more relevant in the electron-positron than in the muon pair case.[2] For the same reason, D-wave resonances are not included. Moreover, we sum over the lowest lying unflavored vector resonances, and thus, for instance, $\rho(1450)^0$ is not included, further limiting the kinematic window to $q^2(\ell^+\ell^-) \lesssim 1.5$ GeV^2. LHCb [2–4] collected plenty of data in the region delimited by the two above conditions, namely, $m^2_{\rho^0} \lesssim q^2(\ell^+\ell^-) \lesssim 1.5$ GeV^2 [no bins simultaneously in both $q^2(\ell^+\ell^-)$ and $p^2(\pi^+\pi^-)$ are provided in their analysis]. We postpone to future work the discussion of isospin-two contributions to the S-wave, which is nonresonant at sufficiently low energies [28], and thus, in particular, its phase motion does not experience a large variation [37]: in practice, it decreases steadily starting from $2m_\pi$ and achieves about $-25°$ at around 1 GeV.

Concerning other rare charm-meson decay modes with pion pairs in the final state, we note that the channel $D^\pm \to \pi^\pm\pi^0\ell^+\ell^-$ is not sensitive to the S-wave contributions under discussion and is experimentally more challenging. The mode $D^0 \to \pi^0\pi^0\ell^+\ell^-$ (which does not receive contributions of the P-wave, following Bose-Einstein symmetry) represents an even more significant experimental challenge. These decay modes will thus not be discussed in the following.

Before concluding this Introduction, let us point out that the S-wave contribution is relevant also in the bottom sector.[3] For a discussion in the case of $B^0 \to K^+\pi^-\ell^+\ell^-$, where the S-wave contamination from $B^0 \to K_0^*(\to K^+\pi^-)\ell^+\ell^-$ in the reconstruction of the decay chain is at the level of ≈10%, see Refs. [46–52]; note that LHCb has performed measurements of the S-wave contribution, e.g., in Refs. [53,54]. In the cases of scalar isoscalar states, the S-wave has been discussed for $B_{(s)} \to \pi\pi J/\psi$ [55–57], which contributes to $B_{(s)} \to \pi\pi\ell^+\ell^-$; note that the σ is expected to provide a sizable contribution, naively as large as ≈26%, and thus coincides with the result of BESIII [29] in the charm-sector, since $\mathcal{B}(B^0 \to \rho^0 J/\psi(1S)) \simeq 2.6 \times 10^{-5}$ [58,59], while $\mathcal{B}(B^0 \to \sigma J/\psi(1S)) \simeq 0.9 \times 10^{-5}$ [58]. A process related to the final state with pion pairs is $B_{(s)} \to KK\ell^+\ell^-$ [46,49,50], due to final-state rescattering [55–57]. In the case of B_s decays, $\mathcal{B}(B_s^0 \to \phi J/\psi(1S)) \simeq 1.04 \times 10^{-3}$ [60], while $\mathcal{B}(B_s^0 \to f_0(980) J/\psi(1S)) \simeq 1.2 \times 10^{-4}$ [61], and thus also a sizable contribution from scalar isoscalar resonances. Important contributions of the S-wave are in principle also to be expected in semileptonic decays $B^+ \to \pi\pi\ell^+\nu_\ell$ ($\ell = e, \mu, \tau$) [62,63], and should then be taken into account in future tests of the SM, such as lepton flavor universality; see Ref. [64] for a discussion of the extraction of the P-wave contribution from a lattice QCD calculation. See Refs. [65–68] for discussions of the S-wave contribution to $\bar{B} \to D\pi\ell^-\bar{\nu}_\ell$.

[2] The differential branching ratio as a function of $p^2(\pi^+\pi^-)$ is dominated by $\ell^+\ell^-$ resonant contributions [i.e., after integration of the fully differential branching ratio over the variable $q^2(\ell^+\ell^-)$], and thus bremsstrahlung represents a correction that we neglect. This is a very good approximation, particularly at low $p^2(\pi^+\pi^-)$ [16].

[3] For the theoretical treatment of $K_{L,S} \to \pi^+\pi^-\ell^+\ell^-$ decays, see Refs. [40–44]; see also Ref. [45] for $K_{\ell 4}$ decays.

This article is organized as follows: in Sec. II we formalize the inclusion of intermediate resonances; then, in Sec. III we discuss the theoretical expressions of distinct observables; finally, in Sec. IV we present our numerical comparisons with available data; conclusions are provided in Sec. V. In Appendix A we give the expressions of the line shapes in use, among further useful hadronic information, and some further comparisons regarding Ref. [29] are given in Appendix B.

II. INCLUSION OF INTERMEDIATE RESONANCES IN NAIVE FACTORIZATION

To start, we introduce the single Cabibbo suppressed (SCS) effective interaction Hamiltonian density for $\Delta C = 1$ up to operators of dimension six, valid for energy scales $\mu < \mu_b$ (μ_b being the energy scale at which the bottom quark is integrated out) [69]:

$$\mathcal{H}_{\rm eff} = \frac{G_F}{\sqrt{2}}\left[\sum_{i=1}^{2} C_i(\mu)(\lambda_d Q_i^d + \lambda_s Q_i^s) - \lambda_b\big(C_7(\mu)Q_7 + C_9(\mu)Q_9 + C_{10}(\mu)Q_{10}\big)\right] + \text{H.c.}, \tag{2}$$

where

$$\lambda_q = V_{cq}^* V_{uq}, \qquad q = d, s, b. \tag{3}$$

The basis of operators is the following:

$$\begin{aligned}
Q_1^d &= (\bar{d}c)_{V-A}(\bar{u}d)_{V-A},\\
Q_2^d &= (\bar{d}_\beta c_\alpha)_{V-A}(\bar{u}_\alpha d_\beta)_{V-A} \overset{Fierz}{=} (\bar{u}c)_{V-A}(\bar{d}d)_{V-A},\\
Q_1^s &= (\bar{s}c)_{V-A}(\bar{u}s)_{V-A},\\
Q_2^s &= (\bar{s}_\beta c_\alpha)_{V-A}(\bar{u}_\alpha s_\beta)_{V-A} \overset{Fierz}{=} (\bar{u}c)_{V-A}(\bar{s}s)_{V-A},\\
Q_7 &= \frac{e}{8\pi^2} m_c \bar{u}\sigma_{\mu\nu}(\mathbf{1}+\gamma_5)F^{\mu\nu}c,\\
Q_9 &= \frac{\alpha_{em}}{2\pi}(\bar{u}\gamma_\mu(\mathbf{1}-\gamma_5)c)(\bar{\ell}\gamma^\mu\ell),\\
Q_{10} &= \frac{\alpha_{em}}{2\pi}(\bar{u}\gamma_\mu(\mathbf{1}-\gamma_5)c)(\bar{\ell}\gamma^\mu\gamma_5\ell),
\end{aligned} \tag{4}$$

where $(V-A)_\mu = \gamma_\mu(\mathbf{1}-\gamma_5)$, α, β are color indices, and $\mu \sim \overline{m}_c(m_c)$ is the renormalization scale. The operators Q_i^q, $q = d$, s, and $i = 1$, 2 are the current-current operators. Above, we have not kept contributions in λ_b other than the electromagnetic dipole Q_7 and the semileptonic interactions Q_9 and Q_{10}, which are kept only for the sake of later convenience. The (short-distance) SM Wilson coefficients C_7, C_9, C_{10}, first generated at one loop via the exchange of electroweak (EW) gauge bosons, are significantly suppressed in the D system [70],[4] and furthermore their contributions are accompanied with a CKM suppression; since $C_{10} \sim 0$ in the SM, we will see that some angular observables approximately vanish (i.e., those based in $I_{5,6,7}$). The main SM contribution to an effective C_9 comes from long-distance dynamics, as it will be discussed later in this section. As stressed in Ref. [17], the latter feature is welcome in the sense that it enhances the sensitivity to NP that contributes to the observables that vanish in the SM, such as having Q_{10} induced by NP which interferes with the large SM long-distance part. Operators of flipped chirality, i.e., Q_7', Q_9', Q_{10}', are not displayed, and are virtually absent in the SM, their contributions being relatively suppressed by m_u/m_c. For all purposes, we take $\lambda_s = -\lambda_d$.

The full decay amplitude of the charm-meson decay is calculated here in the framework of factorization, closely following Ref. [16]. We include in our analysis only the quasi-two-body topologies with the lowest lying intermediate resonances that are indicated in Fig. 2. Therein, the lepton pair originates from one vector meson, namely, ρ^0, ω, or ϕ, coupling to a photon (we neglect cases where one isoscalar hadron couples to two photons due to the small resulting effect, as supported by data (see, e.g., Ref. [72]); similarly, we do not include pseudoscalar resonances in our analysis). The pion pair originates from strong decays of ρ^0, ω, or σ. The latter list does not include the ϕ since we assume the Zweig rule to be at play; i.e., we discard the possibility of a light-quark pair rescattering into $s\bar{s}$. Since the intermediate resonances are electrically neutral, the only operators that contribute in naive factorization are Q_2^q, $q = d, s$. We employ the next-to-leading order (NLO) value $C_2 = -0.40$ in the naive dimensional regularization (NDR) scheme at m_c [69,70].

We write schematically for the S-matrix element of the process:

$$\langle \pi^+\pi^-\ell^+\ell^-|S|D^0\rangle = \langle \pi^+\pi^-\ell^+\ell^-| \int d^4x\, d^4w\, d^4y\, d^4z \times T\{\mathcal{H}_{em}^{\rm lept}(z)\mathcal{H}_{\mathcal{V}\gamma}(y)\mathcal{H}_{\mathcal{R}\pi\pi}(w) \times \mathcal{H}_{D\mathcal{R}\mathcal{V}}(x)\}|D^0\rangle, \tag{5}$$

with electromagnetic interactions given by[5] [73]

[4]Because of the GIM mechanism, there are no short-distance contributions to C_7, C_9, C_{10} above the scale μ_b at one loop (single insertions of current-current operators provide long-distance, effective contributions); C_7, C_9 are generated electromagnetically below μ_b via single insertions of dimension-six four-quark operators, while at one loop C_{10} is generated only via double insertions of dimension-six operators, and thus of higher order in G_F [16] (at two loops, single insertions are possible, but of higher order in electromagnetic interactions [17]). Such is also the case in dineutrino decay modes [71].

[5]Integration by parts has been used to rewrite $\mathcal{H}_{\mathcal{V}\gamma} \propto F_{\mu\nu}(\partial^\mu\mathcal{V}^\nu - \partial^\nu\mathcal{V}^\mu)$ [16], and we employed the gauge condition $\partial^\mu A_\mu = 0$. Moreover, $\mathcal{H}_{em}^{\rm lept}$ consists only of an interaction term and is not gauge invariant.

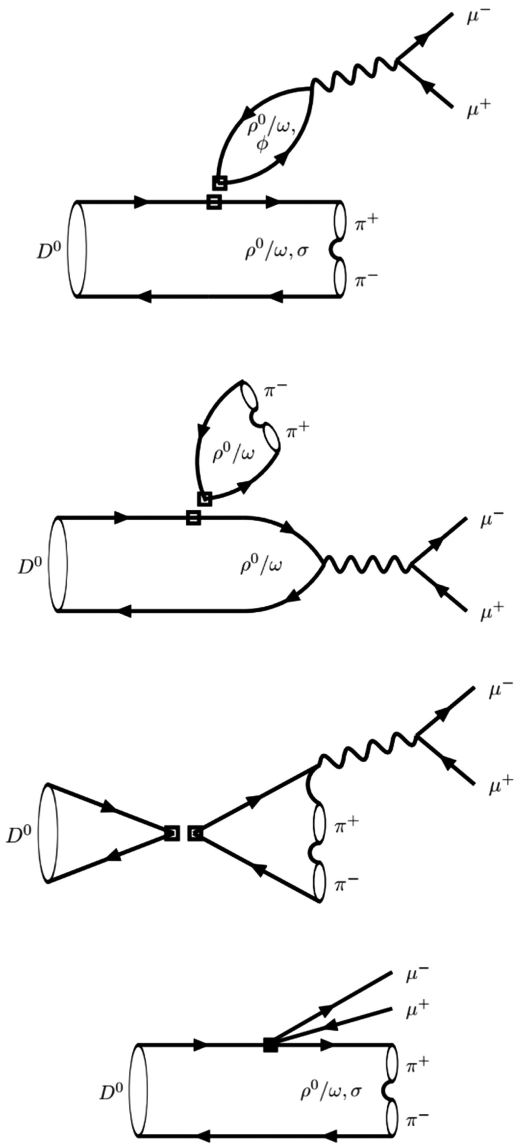

FIG. 2. Quasi-two-body topologies; the lepton (pion) pair comes from electromagnetic (respectively, strong) decays of the intermediate resonances; from top to bottom: W-type factorization contribution, J-type factorization contribution, A-type factorization contribution (i.e., annihilation topology); pairs of empty squares represent the two quark color-neutral bilinears that are factorized. Bottom: contributions for which the lepton pair comes from an effective semileptonic contact interaction, represented by a solid square.

$$\mathcal{H}_{\mathcal{V}\gamma} = -e\left(\frac{f_{\rho^0}}{\sqrt{2}m_{\rho^0}}(\rho^0)^\mu + \frac{1}{3}\frac{f_\omega}{\sqrt{2}m_\omega}\omega^\mu - \frac{\sqrt{2}}{3}\frac{f_\phi}{\sqrt{2}m_\phi}\phi^\mu\right)\Box A_\mu, \qquad \mathcal{H}_{em}^{\mathrm{lept}} = eA^\mu\bar{\ell}\gamma_\mu\ell. \tag{6}$$

Above, $\mathcal{R}$ is one of the vector or scalar resonances coupling to the pion pair, and $\mathcal{V}$ is the vector resonance coupling electromagnetically to the lepton pair. The flavor changing interaction $\mathcal{H}_{D\mathcal{R}\mathcal{V}}$ results from insertions of the current-current operators Q_2^q, $q = d, s$ of the weak Hamiltonian density in Eq. (2), while matrix elements of $\mathcal{H}_{\mathcal{R}\pi\pi}$ are discussed in Secs. II A and II B for intermediate vectors and the scalar, respectively.

Let us at this point define the specific topologies that show up within factorization given the intermediate states aforementioned. There are three possible ways to contract the currents, shown graphically in Fig. 2:

$$\begin{aligned} Q_A &\equiv -\langle\mathcal{R}\mathcal{V}|(\bar{q}q)_{V-A}|0\rangle\langle 0|\bar{u}\gamma^\mu\gamma_5 c|D^0(p_D)\rangle \\ &= \langle\mathcal{R}\mathcal{V}|(\bar{q}q)_A(x)|0\rangle i f_D p_D^\mu e^{-ip_D\cdot x}, \end{aligned} \tag{7}$$

$$Q_W \equiv \begin{cases} \langle\mathcal{V}|(\bar{q}q)_V|0\rangle\langle\mathcal{R}|(\bar{u}c)_{V-A}|D^0\rangle, & \mathcal{R} = \rho^0, \omega, \\ -\langle\mathcal{V}|(\bar{q}q)_V|0\rangle\langle\mathcal{R}|(\bar{u}c)_A|D^0\rangle, & \mathcal{R} = \sigma, \end{cases} \tag{8}$$

$$Q_J \equiv \langle\mathcal{R}|(\bar{q}q)_V|0\rangle\langle\mathcal{V}|(\bar{u}c)_{V-A}|D^0\rangle, \qquad \mathcal{R} = \rho^0, \omega, \tag{9}$$

where $q = d, s$. Both quark bilinears are evaluated at the same spacetime point. Above, we have already indicated explicitly which currents (whether vector, axial-vector, or both) give nonvanishing contributions and which resonances are possible. In particular, note that there is no σ exchange in the Q_J case, since the (axial-)vector $\langle\sigma|(\bar{q}q)_{V(A)}|0\rangle$ matrix element vanishes. The type of contraction at the origin of Q_A, which is the weak annihilation topology, is proportional to the light quark mass m_q, as seen from contracting the axial-vector current $\bar{q}\gamma_\mu\gamma_5 q$ with the decaying charm-meson four-momentum p_D^μ, and we will thus neglect this contribution compared to the other two that are nonzero; see, e.g., Ref. [74] for a discussion.

We are left with the types of contractions of Q_W and Q_J, that we shall refer to as "W"- and "J"-type contractions, and to which we now turn and provide further details. In the case of W-type factorization, we need to evaluate the following vacuum to the lepton pair matrix element:

$$\begin{aligned} &\langle\ell^+\ell^-|\int d^4y\, d^4z\, T\left\{\mathcal{H}_{em}^{\mathrm{lept}}(z)\mathcal{H}_{\mathcal{V}\gamma}(y)\left(\sum_{q=d,s}\lambda_q(\bar{q}q)_V(x)\right)\right\}|0\rangle \\ &= -\sum_{\mathcal{V}=\rho^0,\omega,\phi}\langle\ell^+\ell^-|H_{em}^{\mathrm{lept}}|\gamma^*\rangle\frac{1}{q^2}\langle\gamma^*|H_{\mathcal{V}\gamma}|\mathcal{V}\rangle \\ &\quad\times\frac{1}{P_{\mathcal{V}}(q^2)}\langle\mathcal{V}|\sum_{q=d,s}\lambda_q(\bar{q}q)_V(x)|0\rangle \\ &= -e^{iq\cdot x}\lambda_d e^2(\bar{u}_\ell\gamma^\mu v_\ell)\left(\frac{c_{\rho^0}^W f_{\rho^0}^2}{P_{\rho^0}(q^2)} + \frac{c_\omega^W f_\omega^2}{P_\omega(q^2)} + \frac{c_\phi^W f_\phi^2}{P_\phi(q^2)}\right), \end{aligned} \tag{10}$$

where q^2 is the invariant mass squared of the lepton pair, $c_{\rho^0}^W = 1/2$, $c_\omega^W = -1/6$, and $c_\phi^W = -1/3$. The expressions for the line shapes will be discussed later in the text (see Appendix A 3).[6] Note that the ϕ contribution comes with the CKM factor λ_s, where $\lambda_s = -\lambda_d$. For the values of the decay constants, see Appendix A 1.

In the J-type factorization, we need to evaluate the following $D^0 \to \ell^+\ell^-$ matrix element:

$$\begin{aligned}
&\langle \ell^+\ell^- | \int d^4y\, d^4z T\{\mathcal{H}_{em}^{\rm lept}(z)\mathcal{H}_{\mathcal{V}\gamma}(y)\lambda_d(\bar{u}\gamma_\mu c)(x)\}|D^0(p_D)\rangle \\
&= -\sum_{\mathcal{V}=\rho^0,\omega} \langle \ell^+\ell^-|H_{em}^{\rm lept}|\gamma^*\rangle \frac{1}{q^2}\langle \gamma^*|H_{\mathcal{V}\gamma}|\mathcal{V}\rangle \frac{1}{P_\mathcal{V}(q^2)}\langle \mathcal{V}|\lambda_d(\bar{u}\gamma_\mu c)(x)|D^0(p_D)\rangle \\
&= -e^{i(q-p_D)\cdot x}\lambda_d e^2(\bar{u}_\ell\gamma_\mu v_\ell)\left(\frac{c^J_{\rho^0}f_{\rho^0}}{m_{\rho^0}P_{\rho^0}(q^2)} + \frac{c^J_\omega f_\omega}{m_\omega P_\omega(q^2)} + \frac{c^J_\phi f_\phi}{m_\phi P_\phi(q^2)}\right) \\
&\quad \times \left(A_1(p^2)c_1(q^2,p^2) + A_2(p^2)c_2(q^2,p^2) + V(p^2)c_V(q^2,p^2) + A_0(p^2)c_0(q^2,p^2)\right), \qquad (11)
\end{aligned}$$

where p^2 is the invariant mass squared of the pion pair, $c^J_{\rho^0} = 1/\sqrt{2}$, $c^J_\omega = 1/(3\sqrt{2})$, and $c^J_\phi = 0$. Again, the ϕ does not contribute due to its quark content (similarly, there is no contribution proportional to λ_s). The form factors of $D \to \mathcal{V}$, $\mathcal{V} = \rho^0, \omega$, are equal for the two resonances (see Appendix A 2 for details about their parametrizations); the functions $c_i(q^2, p^2)$, $i = V, 0, 1, 2$, encode the kinematical factors that accompany each form factor [75].

In Eqs. (10) and (11), the relative signs and numerical prefactors between ρ^0 and ω can be quickly understood from the quark content of the vector resonances

$$\begin{aligned}
V_\mu^\phi &\equiv \bar{s}\gamma_\mu s, \\
V_\mu^\omega &\equiv \frac{1}{\sqrt{2}}\left(\bar{u}\gamma_\mu u + \bar{d}\gamma_\mu d\right), \\
V_\mu^{\rho^0} &\equiv \frac{1}{\sqrt{2}}\left(\bar{u}\gamma_\mu u - \bar{d}\gamma_\mu d\right), \qquad (12)
\end{aligned}$$

where the quark content of the operators $V_\mu^\mathcal{V}$ is such that they can create or annihilate the vector meson $\mathcal{V}$, and we enforce the Zweig rule (for corrections, see, e.g., Ref. [76]). In terms of these operators, the hadronic electromagnetic current can be rewritten as

$$\left(j_{em}^{\rm had}\right)_\mu = Q_s V_\mu^\phi + \frac{Q_u + Q_d}{\sqrt{2}}V_\mu^\omega + \frac{Q_u - Q_d}{\sqrt{2}}V_\mu^{\rho^0}, \qquad (13)$$

where $Q_u = +2/3$ and $Q_d = Q_s = -1/3$.

To accommodate further strong dynamics, we will in the following discussion associate a strong phase $\delta_{\{\mathcal{R},\mathcal{V}\}}$ with each vertex $\langle \mathcal{R}\mathcal{V}|\mathcal{H}_{D\mathcal{R}\mathcal{V}}|D^0\rangle$; a similar approach is followed by Ref. [17]; see also Ref. [19] (strong phases are extracted from e^+e^- data in Refs. [19,77]). It will be assumed that these strong phases vary slowly, the faster variations being expected from the line shapes, and one then takes the $\delta_{\{\mathcal{R},\mathcal{V}\}}$ as constants under the assumption that the main resonances needed for phenomenological applications are included in our analysis. Such strong phases are introduced to represent rescattering effects that take place beyond (naive) factorization. This leaves us with six arbitrary phases for the couplings of D^0 to

$$\begin{aligned}
&\{\rho^0/\omega, \rho^0\}, \qquad \{\rho^0/\omega, \omega\}, \qquad \{\rho^0/\omega, \phi\}, \\
&\{\sigma, \rho^0\}, \qquad \{\sigma, \omega\}, \qquad \{\sigma, \phi\} \qquad (14)
\end{aligned}$$

pairs of resonances, where the first state designates the resonance $\mathcal{R}$ that decays to a pion pair, while the second state stands for the resonance $\mathcal{V}$ that decays to a lepton pair. The notation ρ^0/ω means that we have collected together the ρ^0 and the ω leading to the pion pair; in doing so, the three extra phases $\{\omega, \rho^0\}$, $\{\omega, \omega\}$, $\{\omega, \phi\}$ will be exchanged by a single relative phase ϕ_ω that will be introduced in Eq. (19) below.

In practice, we will see that the presently measured $d\Gamma/dq^2$ distribution depends on the phase differences:

$$\begin{aligned}
\Delta_1 &\equiv \delta_{\{\rho^0/\omega,\rho^0\}} - \delta_{\{\rho^0/\omega,\phi\}}, \\
\Delta_2 &\equiv \delta_{\{\rho^0/\omega,\rho^0\}} - \delta_{\{\rho^0/\omega,\omega\}}, \\
\Delta_3 &\equiv \delta_{\{\sigma,\rho^0\}} - \delta_{\{\sigma,\phi\}}, \\
\Delta_4 &\equiv \delta_{\{\sigma,\rho^0\}} - \delta_{\{\sigma,\omega\}}, \qquad (15)
\end{aligned}$$

since S- and P-waves do not interfere in $d\Gamma/dq^2$; given that the ω and ϕ are narrow resonances, $\Delta_1 - \Delta_2$ and $\Delta_3 - \Delta_4$ do not play an important role. On the other hand, when discussing angular observables that depend on the S- and P-waves interference, the following extra phase difference is relevant:

$$\Delta_{SP} \equiv \delta_{\{\sigma,\rho^0\}} - \delta_{\{\rho^0/\omega,\rho^0\}}, \qquad (16)$$

which completes the list of phase differences in the SM to be discussed below: i.e., out of six phases we have five independent differences among them.

[6]We reserve the typesetting $\mathcal{H}$ for the Hamiltonian density, while H denotes the Hamiltonian.

A. Implementation of the $\pi^+\pi^-$ P-wave contribution

For the coupling of a vector resonance V to the pion pair we use the following expression for the matrix element of $H_{\mathcal{R}\pi\pi}$ resulting from strong interactions:

$$\begin{aligned}&\langle \pi^+(p_1)\pi^-(p_2)|H_{\mathcal{R}\pi\pi}|V(p,\lambda)\rangle \\ &\quad = F_{\mathrm{BW}}(p^2) b_V\, \epsilon_V(p,\lambda)\cdot(p_1-p_2), \end{aligned} \tag{17}$$

where the phenomenological form factor F_{BW} is the so-called Blatt-Weisskopf barrier factor for a particle of spin-one; see Appendix A 3 for definitions and the review on resonances of Ref. [28]. The quantity b_V is assumed not to carry any dynamics and is extracted from the decay rate of $V \to \pi^+\pi^-$:

$$\Gamma(V\to\pi^+\pi^-) = \frac{1}{48\pi} b_V^2 m_V^{-5} \lambda^{3/2}(m_V^2, m_\pi^2, m_\pi^2), \tag{18}$$

where $\lambda(a,b,c) = a^2+b^2+c^2-2(ab+bc+ca)$. In practice this relation is used only for $V=\rho^0$, for which we take $\mathcal{B}(\rho^0\to\pi^+\pi^-)=1$, thus resulting in $b_{\rho^0}=5.92$.

The line shape of ρ^0 is expressed in the Gounaris-Sakurai parametrization [78], which implements finite-width corrections (see Appendix A 3 for details). Following previous literature on ρ^0/ω contributions to $e^+e^-\to\pi^+\pi^-$, we collect both resonances together by considering the expression

$$b_{\rho^0/\omega}(p^2) = b_{\rho^0}\left(1 + a_\omega e^{i\phi_\omega}\mathrm{RBW}_\omega(p^2)\right), \tag{19}$$

where the relativistic Breit-Wigner (RBW) line shape $\mathrm{RBW}_\omega(s)$ is given in Appendix A 3. In (naive) factorization, if only the W-type contraction were possible, then $\phi_\omega = 0$; on the contrary, in the J-type contraction, $\phi_\omega=\pi$. In Eq. (19), both contributions are collected together, and the phase ϕ_ω will also accommodate further hadronic effects beyond (naive) factorization in our study. In Sec. IV, the parameters a_ω and ϕ_ω of the coupling of the ω to two pions are fitted to the experimental differential branching ratio as a function of the invariant mass of the pion pair (a small but nonvanishing value of a_ω is generated from isospin-breaking effects, mixing the isospin-triplet ρ and the isospin-singlet ω states). This is different from the implementation of the resonances in the matrix elements of the lepton pair, where the ρ^0 and ω contributions are added serially. We then have for the contribution where the pion pair originates from ρ^0/ω resonances

$$\begin{aligned}
\langle \pi^+\pi^-\ell^+\ell^-|S|D^0\rangle^{(\rho^0/\omega)} &= (2\pi)^4\delta^{(4)}(p+q-p_D)\xi_2 \frac{b_{\rho^0/\omega}(p^2)F_{\mathrm{BW}}(p^2)}{P_{\rho^0}(p^2)}(\bar{u}_\ell\gamma_\mu v_\ell)\sum_{\mathcal{V}}\left\{\left[\frac{c^W_{\mathcal{V}}B_{\mathcal{V}}f^2_{\mathcal{V}}e^{i\delta_{\{\rho^0/\omega,\mathcal{V}\}}}}{P_{\mathcal{V}}(q^2)}\right.\right.\\
&\quad\times\left(\frac{2q\cdot(p_1-p_2)}{m_D+\sqrt{p^2}}A_2(q^2) - (m_D+\sqrt{p^2})A_1(q^2)\right) + \frac{1}{\sqrt{2}}m_{\rho^0}f_{\rho^0}\frac{c^J_{\mathcal{V}}B_{\mathcal{V}}f_{\mathcal{V}}e^{i\delta_{\{\rho^0/\omega,\mathcal{V}\}}}}{m_{\mathcal{V}}P_{\mathcal{V}}(q^2)}\\
&\quad\times\left.\left(\frac{2q\cdot(p_1-p_2)}{m_D+\sqrt{q^2}}A_2(p^2) - (m_D+\sqrt{q^2})A_1(p^2)\right)\right]p_1^\mu + \left[\frac{c^W_{\mathcal{V}}B_{\mathcal{V}}f^2_{\mathcal{V}}e^{i\delta_{\{\rho^0/\omega,\mathcal{V}\}}}}{P_{\mathcal{V}}(q^2)}\right.\\
&\quad\times\left(\frac{2q\cdot(p_1-p_2)}{m_D+\sqrt{p^2}}A_2(q^2) + (m_D+\sqrt{p^2})A_1(q^2)\right) + \frac{1}{\sqrt{2}}m_{\rho^0}f_{\rho^0}\frac{c^J_{\mathcal{V}}B_{\mathcal{V}}f_{\mathcal{V}}e^{i\delta_{\{\rho^0/\omega,\mathcal{V}\}}}}{m_{\mathcal{V}}P_{\mathcal{V}}(q^2)}\\
&\quad\times\left.\left(\frac{2q\cdot(p_1-p_2)}{m_D+\sqrt{q^2}}A_2(p^2) + (m_D+\sqrt{q^2})A_1(p^2)\right)\right]p_2^\mu + \left[\frac{c^W_{\mathcal{V}}B_{\mathcal{V}}f^2_{\mathcal{V}}e^{i\delta_{\{\rho^0/\omega,\mathcal{V}\}}}}{P_{\mathcal{V}}(q^2)}\frac{-4iV(q^2)}{m_D+\sqrt{p^2}}\right.\\
&\quad\left.\left.+\frac{1}{\sqrt{2}}m_{\rho^0}f_{\rho^0}\frac{c^J_{\mathcal{V}}B_{\mathcal{V}}f_{\mathcal{V}}e^{i\delta_{\{\rho^0/\omega,\mathcal{V}\}}}}{m_{\mathcal{V}}P_{\mathcal{V}}(q^2)}\frac{-4iV(p^2)}{m_D+\sqrt{q^2}}\right]\epsilon^{\mu\nu\lambda\rho}p_{1\nu}p_{2\lambda}q_\rho\right\},
\end{aligned} \tag{20}$$

where

$$\xi_2 = \lambda_d \frac{G_F}{\sqrt{2}} e^2 C_2(\mu). \tag{21}$$

The terms coming with $A_1(q^2)$, $A_2(q^2)$, $V(q^2)$ [respectively, $A_1(p^2)$, $A_2(p^2)$, $V(p^2)$] originate from the W-type (J-type) factorization, since the momentum transfer of the D^0 form factor is the one of the lepton pair (pion pair).[7] Note that the A_0 contribution vanishes because it is accompanied by $q^\mu\bar{\ell}\gamma_\mu\ell=0$ in the W-type factorization, and by $p_1^2-p_2^2$ in the J-type factorization, also vanishing in the case of $\pi^+\pi^-$ final-state mesons. In the case of

[7] In the above we have used the approximation $m_\omega f_\omega \approx m_{\rho^0}f_{\rho^0}$ for the $0\to V$ term in the J-type factorization, in order to simplify the expression.

charm-meson decays the J-type contribution gives sizable effects, as it is manifest from Eq. (20).[8]

In Eq. (20), apart from the complex phases that correct the (naive) factorization picture, we have also introduced for the same reason the real and positive parameters B_{ρ^0}, B_ω, and B_ϕ that will be adjusted from data, and are also assumed not to carry any dependence with the energy. Note that a somewhat similar approach is followed by Ref. [17], which fits the factors controlling the normalizations of the resonances around their respective peaks.

B. Implementation of the $\pi^+\pi^-$ S-wave contribution

We now consider the effect of the $\sigma = f_0(500)$ resonance. The σ is encoded in the w_+ and r form factors of the $D^0 \to \pi^+\pi^-$ matrix element [75,79,80]:

$$\begin{aligned}&\langle \pi^+(p_1)\pi^-(p_2)|(\bar{u}\gamma^\mu(1-\gamma_5)c)(x)|D^0(p_D)\rangle\\&= e^{ix\cdot(p-p_D)}\{iw_+(p_1+p_2)^\mu + iw_-(p_1-p_2)^\mu\\&\quad + h\epsilon^{\mu\alpha\beta\gamma}(p_D)_\alpha(p_1+p_2)_\beta(p_1-p_2)_\gamma + irq^\mu\}. \end{aligned} \tag{22}$$

The contraction of q^μ with the spinorial part of the leptonic matrix element $(\bar{u}_\ell\gamma^\mu v_\ell)$ in Eq. (10) vanishes, and thus the effect of the S-wave intermediate states appears only in the form factor w_+, to which the following S-wave term is added:

$$\begin{aligned}w_+^S(p^2,q^2) &= a_S(q^2)\mathcal{A}_S(p^2),\\ a_S(q^2) &= a_S(0)/\left(1-\frac{q^2}{m_A^2}\right).\end{aligned} \tag{23}$$

Here, the nearest pole is used [29], for which we have $m_A = 2.42$ GeV, where A is the axial D-meson ($J^P = 1^+$). The quantity $a_S(0)$, assumed to be a constant,[9] represents a magnitude encompassing the strength of the transition $D \to \sigma$ multiplied by the coupling of σ to the pion pair. We extract it from fitting the experimental data. Following Ref. [29], the line shape $\mathcal{A}_S(p^2)$ is the one of Bugg [26], which is data driven (and in particular includes small Zweig-violating effects); its full expression is provided in Appendix A 3. The complex phase assigned to the σ is close to the one extracted from $\pi\pi$ rescattering in the elastic region. We reserve the analysis of alternative line shapes to the future when the quest for higher precision may become more pressing.

With all the above, we incorporate the scalar resonance to our factorization model

$$\begin{aligned}\langle \pi^+\pi^-\ell^+\ell^-|S|D^0\rangle^{(\sigma)} &= (2\pi)^4\delta^{(4)}(p+q-p_D)\\&\quad\times \xi_2(\bar{u}_\ell\gamma_\mu v_\ell)i\sum_{\mathcal{V}}\frac{c_{\mathcal{V}}^W B_{\mathcal{V}}^{(S)} f_{\mathcal{V}}^2 e^{i\delta_{\{\sigma,\mathcal{V}\}}}}{P_{\mathcal{V}}(q^2)}\\&\quad\times a_S(q^2)\mathcal{A}_S(p^2).\end{aligned} \tag{24}$$

The full matrix element is then given by

$$\begin{aligned}\langle \pi^+\pi^-\ell^+\ell^-|S|D^0\rangle &= \langle \pi^+\pi^-\ell^+\ell^-|S|D^0\rangle^{(\rho^0/\omega)}\\&\quad+\langle \pi^+\pi^-\ell^+\ell^-|S|D^0\rangle^{(\sigma)}.\end{aligned} \tag{25}$$

C. Effective Wilson coefficient

It would be useful to write the previous matrix element in Eq. (25) as the matrix element of a semileptonic four-fermion operator, with the intermediate resonance at the origin of the lepton pair encoded in an effective Wilson coefficient. Assuming that the only factorization is the W-type one, as is the case, for instance, in semileptonic nonrare decays, it is easy to match the full hadronic matrix element to that of a Q_9 operator, i.e., in which the quark pair carries the chiral $V-A$ structure, and the lepton pair a vector structure, as it would result from the coupling to a single photon. As seen from Eqs. (8) and (10), the matrix element $\langle \pi^+\pi^-|(\bar{u}c)_{V-A}(x)|D^0\rangle$ for initial and final-state mesons has been factorized out from the leptonic matrix element, and we are able to write the latter as $\langle \ell^+\ell^-|(\bar{\ell}\ell)_V(x)|0\rangle$ times an effective coefficient that encodes the intermediate resonant dynamics of the lepton pair invariant mass

$$\begin{aligned}C_9^{\mathrm{eff}:W}(\mu;q^2) = 8\pi^2 C_2(\mu)\Bigg(&\frac{c_{\rho^0}^W f_{\rho^0}^2}{P_{\rho^0}(q^2)}B_{\rho^0}e^{i\delta_{\{\rho^0/\omega,\rho^0\}}}\\&+\frac{c_\omega^W f_\omega^2}{P_\omega(q^2)}B_\omega e^{i\delta_{\{\rho^0/\omega,\omega\}}}+\frac{c_\phi^W f_\phi^2}{P_\phi(q^2)}B_\phi e^{i\delta_{\{\rho^0/\omega,\phi\}}}\Bigg)\end{aligned} \tag{26}$$

[where we have included the factors beyond (naive) factorization that have been previously discussed], such that the transition $c \to u\ell^+\ell^-$ is described by

$$\mathcal{H}_{\mathrm{eff}}^{c\to u\ell\ell} = \frac{G_F}{\sqrt{2}}\lambda_d C_9^{\mathrm{eff}:W}(\mu;q^2)Q_9 + \mathrm{H.c.} \tag{27}$$

In writing Eq. (26), we consider only the P-wave, while the S-wave will be discussed shortly below.

Conversely, the matrix element appearing in the J-type contribution is $\langle \mathcal{V}|(\bar{u}c)_{V-A}|D^0\rangle$, where $\mathcal{V}$ does not lead to the pion pair, but instead to the lepton pair, so we cannot separate the full matrix element into hadronic times leptonic factors calculated at the same spacetime point.

[8]The analogous J-type contribution in $B^+ \to K^{(*)+}\ell^+\ell^-$ transitions from current-current operators is $V_{ub}^*V_{us}$-suppressed with respect to the dominant contribution, which goes as $V_{cb}^*V_{cs}$.

[9]A dynamical behavior of $a_S(0)$ could, for instance, result from the annihilation topology.

Thus, this contribution prevents us from writing, at least straightforwardly, our full amplitude using an effective Wilson coefficient multiplying a semileptonic four-fermion operator.

In the following we explore an alternative that would make the use of an approximate effective C_9 coefficient viable if the ρ^0/ω were the only resonances creating the pion pair. Starting with the ρ^0, we rewrite the J- and W-type contributions in a similar way. By inspecting Eq. (20), one condition is that

$$m_{\rho^0} f_{\rho^0} \frac{f_{\rho^0}}{m_{\rho^0} P_{\rho^0}(q^2)} \frac{1}{m_D + \sqrt{q^2}} F(p^2) \simeq \frac{f_{\rho^0}^2}{P_{\rho^0}(q^2)} \frac{1}{m_D + \sqrt{p^2}} F(q^2), \qquad F = A_2, V, \tag{28}$$

while a similar discussion holds for the terms that are proportional to the form factor A_1. To achieve our goal, we need first to examine if the $m_D + \sqrt{q^2}$ and $m_D + \sqrt{p^2}$ factors can be replaced with $m_D + m_\rho$, as it is usually done in the literature. Indeed, this narrow-width approximation is good enough. What is left of the above conditions in Eq. (28) comes from the dependencies of the form factors on q^2 or p^2. Since in our nearest pole parametrization of the form factors in Appendix A 2 these dependencies go as $m_{\rm pole}^2/(m_{\rm pole}^2 - q^2)$ or $m_{\rm pole}^2/(m_{\rm pole}^2 - p^2)$, and the dilepton and dihadron invariant masses are generally much smaller than the pole masses, the two dependencies are soft.

The situation is more complicated for the ω. Since c_ω^W and c_ω^J have opposite signs, seemingly the ω contribution in the leptonic part would disappear in Eq. (20) under the use of the simplifications discussed in the previous paragraph. However, when considering the original picture before the introduction of $b_{\rho^0/\omega}(p^2)$ in Eq. (19),

$$b_{\rho^0}\left(1 + a_\omega \mathrm{RBW}_\omega(p^2)\right) c_\omega^W \frac{f_\omega^2}{P_\omega(q^2)} \tag{29}$$

from the W-type and

$$b_{\rho^0}\left(1 - a_\omega \mathrm{RBW}_\omega(p^2)\right) \frac{1}{\sqrt{2}} c_\omega^J \frac{f_\omega^2}{P_\omega(q^2)} \tag{30}$$

from the J-type factorization, we see that an $\omega \to \ell^+\ell^-$ contribution survives in the form of

$$b_{\rho^0} a_\omega \mathrm{RBW}_\omega(p^2) \left(c_\omega^W - \frac{1}{\sqrt{2}} c_\omega^J\right) \frac{f_\omega^2}{P_\omega(q^2)}; \tag{31}$$

i.e., the contributions $D^0 \to [\rho^0 \to \pi^+\pi^-]\omega$ from the W- and the J-type terms largely cancel in naive factorization, while the surviving $D^0 \to [\omega \to \pi^+\pi^-]\omega$ contributions are suppressed due to the smallness of the factor a_ω coming from the small coupling of $\omega \to \pi\pi$. Finally, the ω term is introduced in the effective Wilson coefficient with a small parameter $\epsilon_\omega \equiv a_\omega \mathrm{RBW}_\omega(p^2)$, where the dependence on p^2 is not soft as in the previous paragraph. The presence of a p^2 dependence represents an impediment for the introduction of an effective C_9 coefficient, which should apply simultaneously for both ρ^0 and ω decays to a pion pair in the presence of both W- and J-type topologies; however, this represents only a small effect, suppressed by a_ω.

Under all of the above simplifications, one is able to define an approximate effective coefficient for Q_9 containing P-wave contributions as

$$\begin{aligned} C_9^{\mathrm{eff}:P}(\mu; q^2) = 8\pi^2 C_2(\mu) & \\ \times \Bigg[& \left(c_{\rho^0}^W + \frac{1}{\sqrt{2}} c_{\rho^0}^J\right) \frac{f_{\rho^0}^2}{P_{\rho^0}(q^2)} B_{\rho^0} e^{i\delta_{\{\rho^0/\omega,\rho^0\}}} \\ & + \left(c_\omega^W - \frac{1}{\sqrt{2}} c_\omega^J\right) \frac{f_\omega^2}{P_\omega(q^2)} B_\omega \epsilon_\omega e^{i\delta_{\{\rho^0/\omega,\omega\}}} \\ & + c_\phi^W \frac{f_\phi^2}{P_\phi(q^2)} B_\phi e^{i\delta_{\{\rho^0/\omega,\phi\}}} \Bigg], \end{aligned} \tag{32}$$

where the p^2 dependence is omitted in ϵ_ω, which as previously stressed represents a suppression factor. In contrast, the W- and J-type contributions add up coherently in the case of the $D^0 \to [\rho^0 \to \pi^+\pi^-]\rho^0$ contribution and are unsuppressed. We remind the reader that there is no J-type contribution for the ϕ, i.e., $c_\phi^J = 0$. Therefore, we have for the S-matrix element of the process

$$\begin{aligned} \langle \pi^+\pi^-\ell^+\ell^-|S|D^0\rangle^{(\rho^0/\omega)} \simeq (2\pi)^4 \delta^{(4)}(p + q - p_D) & \\ \times C_9^{\mathrm{eff}:P}(\mu; q^2) \langle \pi^+\pi^-\ell^+\ell^-| & \\ \times Q_9 |D^0\rangle^{(\rho^0/\omega)}, & \end{aligned} \tag{33}$$

which should be sufficient for our purposes given the present level of experimental accuracy in the high-energy window of Fig. 1.

For the σ, the discussion is simpler, since there is no J-type contribution:

$$\begin{aligned} \langle \pi^+\pi^-\ell^+\ell^-|S|D^0\rangle^{(\sigma)} = (2\pi)^4 \delta^{(4)}(p + q - p_D) & \\ \times C_9^{\mathrm{eff}:S}(\mu; q^2) \langle \pi^+\pi^-\ell^+\ell^-| & \\ \times Q_9 |D^0\rangle^{(\sigma)}, & \end{aligned} \tag{34}$$

with the $C_9^{\mathrm{eff}:S}$ given by

$$C_9^{\mathrm{eff}:S}(\mu;q^2) = 8\pi^2 C_2(\mu)\left(\frac{c^W_{\rho^0} f^2_{\rho^0}}{P_{\rho^0}(q^2)} B^{(S)}_{\rho^0} e^{i\delta_{\{\sigma,\rho^0\}}} + \frac{c^W_\omega f^2_\omega}{P_\omega(q^2)} B^{(S)}_\omega e^{i\delta_{\{\sigma,\omega\}}} + \frac{c^W_\phi f^2_\phi}{P_\phi(q^2)} B^{(S)}_\phi e^{i\delta_{\{\sigma,\phi\}}}\right). \tag{35}$$

Because of the cancellation discussed above, around Eq. (31), the main contribution underlying $\omega \to \ell^+\ell^-$ is the one paired with $\sigma \to \pi^+\pi^-$. Were the J-type contraction not considered, this would spoil the assessment from the fits of the size of the contribution $D^0 \to [\sigma \to \pi^+\pi^-] \times [\omega \to \ell^+\ell^-]$. Note that $B_{\rho^0}, B_\omega, B_\phi$ in Eq. (32) for the P-wave are allowed to be different with respect to Eq. (35) for the S-wave [moreover, an overall relative scale between P- and S-waves will be absorbed into $a_S(0)$ by setting $B_{\rho^0} = B^{(S)}_{\rho^0}$].

Finally, we have

$$\begin{aligned}
&\langle \pi^+\pi^-\ell^+\ell^-|S|D^0\rangle \\
&\simeq (2\pi)^4\delta^{(4)}(p+q-p_D)(C_9^{\mathrm{eff}:P}(\mu;q^2) \\
&\quad\times \langle \pi^+\pi^-\ell^+\ell^-|Q_9|D^0\rangle^{(\rho^0/\omega)} + C_9^{\mathrm{eff}:S}(\mu;q^2) \\
&\quad\times \langle \pi^+\pi^-\ell^+\ell^-|Q_9|D^0\rangle^{(\sigma)}),
\end{aligned} \tag{36}$$

which, due to the J-type contraction and effects beyond naive factorization, is *not* proportional to

$$\langle \pi^+\pi^-\ell^+\ell^-|Q_9|D^0\rangle \equiv \langle \pi^+\pi^-\ell^+\ell^-|Q_9|D^0\rangle^{(\rho^0/\omega)} + \langle \pi^+\pi^-\ell^+\ell^-|Q_9|D^0\rangle^{(\sigma)}. \tag{37}$$

As previously announced, this prevents us from writing an effective coefficient that would apply simultaneously for both the intermediate P- and S-waves of the pion pair.

For our numerical results we use the full formulas with W- and J-type factorizations. Nevertheless, for the sake of greatly simplifying the presentation of formulas in the next section, while keeping a good numerical accuracy, we employ the notation $C_9^{\mathrm{eff}:P}$ and $C_9^{\mathrm{eff}:S}$ introduced above.

III. DIFFERENTIAL BRANCHING RATIOS AND ANGULAR OBSERVABLES

A set of angular observables can be defined by integrating the differential decay rate of the process over the angular kinematical variables $\theta_\pi, \theta_\ell, \phi$: θ_ℓ is the angle between the ℓ^--momentum and the D-momentum in the dilepton center of mass frame, θ_π is the angle between the π^+-momentum and the negative D-momentum in the dipion center of mass frame, and ϕ is the angle between the dilepton and dipion decay planes, oriented according to the normal vectors $\hat{n}_\ell$ and $\hat{n}_\pi$ of the planes $(\ell^-\ell^+)$ and $(\pi^+\pi^-)$ in the D center of mass frame, respectively, from $\hat{n}_\ell$ to $\hat{n}_\pi$; with respect to Refs. [2–4], our angle ϕ differs by π (which means that the observables based on I_4, I_5, I_7, I_8 flip signs). The total decay rate can be written as

$$\frac{d^5\Gamma}{dq^2dp^2d\Omega} = \frac{1}{2\pi}\sum_{i=1}^{9} c_i I_i, \tag{38}$$

where $d\Omega = d\cos\theta_\pi d\cos\theta_\ell d\phi$ and the constants c_i are

$$\begin{aligned}
&c_1 = 1, \qquad c_2 = \cos 2\theta_\ell, \qquad c_3 = \sin^2\theta_\ell \cos 2\phi, \\
&c_4 = \sin 2\theta_\ell \cos\phi, \qquad c_5 = \sin\theta_\ell\cos\phi, \\
&c_6 = \cos\theta_\ell, \qquad c_7 = \sin\theta_\ell \sin\phi, \\
&c_8 = \sin 2\theta_\ell \sin\phi, \qquad c_9 = \sin^2\theta_\ell \sin 2\phi.
\end{aligned} \tag{39}$$

We present the expressions for the coefficients I_i in terms of the long-distance transversity form factors, the effective Wilson coefficients in the SM, distinguishing between the S- and the P-wave mediated cases, and the local Wilson coefficients introduced by NP. We follow closely the discussion of Refs. [16,17,50].[10] Their expressions are as follows (the integrals $\langle\cdot\rangle_\pm$ over θ_π will be defined below):

$$\begin{aligned}
I_1 &= \frac{1}{8}\Big[|\mathcal{F}_S|^2\rho^-_{1,S} + \cos^2\theta_\pi|\mathcal{F}_P|^2\rho^-_{1,P} \\
&\quad + \frac{3}{2}\sin^2\theta_\pi\big\{|\mathcal{F}_\parallel|^2\rho^-_{1,P} + |\mathcal{F}_\perp|^2\rho^+_{1,P}\big\}\Big] + \langle I_1\rangle_- \cos\theta_\pi \\
&\xrightarrow{\mathrm{SM}} + \frac{1}{8}\Big\{\Big[\cos^2\theta_\pi|\mathcal{F}_P|^2 + \frac{3}{2}\sin^2\theta_\pi\{|\mathcal{F}_\parallel|^2 + |\mathcal{F}_\perp|^2\}\Big] \\
&\quad\times |C_9^{\mathrm{eff}:P}|^2 + |\mathcal{F}_S|^2|C_9^{\mathrm{eff}:S}|^2 \\
&\quad + 2\mathrm{Re}\big\{\mathcal{F}_S\mathcal{F}_P^* C_9^{\mathrm{eff}:S}(C_9^{\mathrm{eff}:P})^*\big\}\cos\theta_\pi\Big\},
\end{aligned} \tag{40}$$

$$\begin{aligned}
I_2 &= -\frac{1}{8}\Big[|\mathcal{F}_S|^2\rho^-_{1,S} + \cos^2\theta_\pi|\mathcal{F}_P|^2\rho^-_{1,P} \\
&\quad - \frac{1}{2}\sin^2\theta_\pi\big\{|\mathcal{F}_\parallel|^2\rho^-_{1,P} + |\mathcal{F}_\perp|^2\rho^+_{1,P}\big\}\Big] + \langle I_2\rangle_- \cos\theta_\pi \\
&\xrightarrow{\mathrm{SM}} - \frac{1}{8}\Big\{\Big[\cos^2\theta_\pi|\mathcal{F}_P|^2 - \frac{1}{2}\sin^2\theta_\pi\{|\mathcal{F}_\parallel|^2 + |\mathcal{F}_\perp|^2\}\Big] \\
&\quad\times |C_9^{\mathrm{eff}:P}|^2 + |\mathcal{F}_S|^2|C_9^{\mathrm{eff}:S}|^2 \\
&\quad + 2\mathrm{Re}\big\{\mathcal{F}_S\mathcal{F}_P^* C_9^{\mathrm{eff}:S}(C_9^{\mathrm{eff}:P})^*\big\}\cos\theta_\pi\Big\},
\end{aligned} \tag{41}$$

[10]We correct Eq. (A.6) from Appendix A of Ref. [16], considering the conventions for the angles specified above; also, $\epsilon_{0123} = -1$.

$$I_3 = \frac{1}{8}[|\mathcal{F}_\perp|^2\rho_{1,P}^+ - |\mathcal{F}_\parallel|^2\rho_{1,P}^-]\sin^2\theta_\pi \xrightarrow{\text{SM}} \frac{1}{8}[|\mathcal{F}_\perp|^2 - |\mathcal{F}_\parallel|^2]\sin^2\theta_\pi |C_9^{\text{eff}:P}|^2, \tag{42}$$

$$I_4 = \cos\theta_\pi\sin\theta_\pi\frac{3}{2}\langle I_4\rangle_- + \sin\theta_\pi\frac{2}{\pi}\langle I_4\rangle_+ \xrightarrow{\text{SM}} -\frac{1}{4}\text{Re}\{\mathcal{F}_P\mathcal{F}_\parallel^*\}\cos\theta_\pi\sin\theta_\pi|C_9^{\text{eff}:P}|^2 - \frac{1}{4}\text{Re}\{\mathcal{F}_S\mathcal{F}_\parallel^* C_9^{\text{eff}:S}(C_9^{\text{eff}:P})^*\}\sin\theta_\pi, \tag{43}$$

$$I_5 = \cos\theta_\pi\sin\theta_\pi\frac{3}{2}\langle I_5\rangle_- + \sin\theta_\pi\frac{2}{\pi}\langle I_5\rangle_+ \xrightarrow{\text{SM}} 0, \tag{44}$$

$$I_6 = -[\text{Re}\{\mathcal{F}_\parallel\mathcal{F}_\perp^*\}\text{Re}\rho_2^+ + \text{Im}\{\mathcal{F}_\parallel\mathcal{F}_\perp^*\}\text{Im}\rho_2^-]\sin^2\theta_\pi \xrightarrow{\text{SM}} 0, \tag{45}$$

$$I_7 = \cos\theta_\pi\sin\theta_\pi\frac{3}{2}\langle I_7\rangle_- + \sin\theta_\pi\frac{2}{\pi}\langle I_7\rangle_+ \xrightarrow{\text{SM}} 0, \tag{46}$$

$$I_8 = \cos\theta_\pi\sin\theta_\pi\frac{3}{2}\langle I_8\rangle_- + \sin\theta_\pi\frac{2}{\pi}\langle I_8\rangle_+ \xrightarrow{\text{SM}} -\cos\theta_\pi\sin\theta_\pi\frac{1}{4}\text{Im}(\mathcal{F}_P\mathcal{F}_\perp^*)|C_9^{\text{eff}:P}|^2 - \frac{1}{4}\sin\theta_\pi\text{Im}\{\mathcal{F}_S\mathcal{F}_\perp^* C_9^{\text{eff}:S}(C_9^{\text{eff}:P})^*\}, \tag{47}$$

$$I_9 = \frac{1}{2}\left[\text{Re}\{\mathcal{F}_\perp\mathcal{F}_\parallel^*\}\text{Im}\rho_2^+ + \text{Im}\{\mathcal{F}_\perp\mathcal{F}_\parallel^*\}\text{Re}\rho_2^-\right]\sin^2\theta_\pi \xrightarrow{\text{SM}} \frac{\text{Im}\{\mathcal{F}_\perp\mathcal{F}_\parallel^*\}}{4}\sin^2\theta_\pi|C_9^{\text{eff}:P}|^2. \tag{48}$$

The 0-transversity form factor is

$$\mathcal{F}_0 = \mathcal{F}_S + \mathcal{F}_P\cos\theta_\pi; \tag{49}$$

the P-wave form factors can be expressed as

$$\begin{aligned}
\mathcal{F}_P &= -N\frac{b_{\rho^0/\omega}(p^2)F_{\text{BW}}(p^2)\sqrt{\beta_\ell(3-\beta_\ell^2)}\lambda_h^{3/4}\lambda_D^{1/4}}{P_{\rho^0}(p^2)}\frac{(m_D+m_{\rho^0})^2(m_D^2-p^2-q^2)A_1(q^2)-\lambda_D A_2(q^2)}{2\sqrt{2}(m_D+m_{\rho^0})(p^2)^{3/2}},\\
\mathcal{F}_\parallel &= N\frac{b_{\rho^0/\omega}(p^2)F_{\text{BW}}(p^2)\sqrt{\beta_\ell(3-\beta_\ell^2)}\lambda_h^{3/4}\lambda_D^{1/4}}{P_{\rho^0}(p^2)}\frac{\sqrt{q^2}(m_D+m_{\rho^0})A_1(q^2)}{\sqrt{2}p^2},\\
\mathcal{F}_\perp &= -N\frac{b_{\rho^0/\omega}(p^2)F_{\text{BW}}(p^2)\beta_\ell^{3/2}\lambda_h^{3/4}\lambda_D^{3/4}}{P_{\rho^0}(p^2)}\frac{\sqrt{q^2}V(q^2)}{(m_D+m_{\rho^0})p^2},
\end{aligned}\tag{50}$$

while for the S-wave

$$\mathcal{F}_S = -N\frac{\sqrt{\beta_\ell(3-\beta_\ell^2)}\lambda_h^{1/4}\lambda_D^{3/4}}{P_{\text{Bugg}}(p^2)}\frac{a_S(q^2)}{2\sqrt{2}\sqrt{p^2}}, \tag{51}$$

where $P_{\text{Bugg}}(p^2) = 1/\mathcal{A}_S(p^2)$. The kinematic factors appearing in these expressions are $\lambda_h = \lambda(p^2, m_\pi^2, m_\pi^2)$, $\lambda_D = \lambda(m_D^2, p^2, q^2)$, $\beta_\ell = \sqrt{1-4m_\ell^2/q^2}$. The overall normalization is

$$N = \frac{\alpha_{em}G_F\lambda_d}{128\pi^{7/2}m_D^{3/2}}, \tag{52}$$

owing to Eq. (27).

The Wilson coefficients, effective or not, are encoded in

$$\begin{aligned}
\rho_{1,S}^- &= |C_9^{\text{eff}:S} + C_9^{\text{NP}} - C_9'|^2 + |C_{10} - C_{10}'|^2,\\
\rho_{1,P}^\pm &= |C_9^{\text{eff}:P} + C_9^{\text{NP}} \pm C_9'|^2 + |C_{10} \pm C_{10}'|^2,\\
\delta\rho &= \text{Re}\left[(C_9^{\text{eff}:P} + C_9^{\text{NP}} - C_9')(C_{10} - C_{10}')^*\right],\\
\text{Re}\rho_2^+ &= \text{Re}\left[(C_9^{\text{eff}:P} + C_9^{\text{NP}})C_{10}^* - C_9' C_{10}'^*\right],\\
\text{Im}\rho_2^+ &= \text{Im}\left[C_{10}' C_{10}^* + C_9'(C_9^{\text{eff}:P} + C_9^{\text{NP}})^*\right],\\
\text{Re}\rho_2^- &= \frac{1}{2}\left(|C_{10}|^2 - |C_{10}'|^2 + |C_9^{\text{eff}:P} + C_9^{\text{NP}}|^2 - |C_9'|^2\right),\\
\text{Im}\rho_2^- &= \text{Im}\left[C_{10}'(C_9^{\text{eff}:P} + C_9^{\text{NP}})^* - C_{10} C_9'^*\right]
\end{aligned}\tag{53}$$

[as seen from the contributing currents in Eq. (8), a $\rho_{1,S}^+$ analogously defined does not show up]. The SM contribution comes from $C_9^{\text{eff}:S}$ and $C_9^{\text{eff}:P}$, while NP is at the origin of possibly large Wilson coefficients of the operators Q_9', Q_{10}, Q_{10}'; NP could also contribute to Q_9. Inspecting

Eq. (53), note that $\mathrm{Im}\rho_2^\pm$ vanish in the absence of having simultaneously the presences of $V-A$ and $V+A$ structures of the quark bilinears; these same combinations of Wilson coefficients vanish when no CP-violating phase is present; $\delta\rho$, $\mathrm{Re}\rho_2^+$, and $\mathrm{Im}\rho_2^-$ vanish in the absence of having simultaneously the presences of V and A structures of the lepton bilinears. Since we will focus on the high-q^2 energy window of Fig. 1, we will not discuss Q_7 and Q_7' operators. Note, however, that part of the same SM background in the mode $D\to PP+[V'\to\gamma^*\to\ell^+\ell^-]$ also manifests in radiative decays (e.g., $D\to PP+[V'\to\gamma]$, where compared to the semileptonic case one has a real photon). These decay modes would provide additional information on the contributions from dipole operators; see, e.g., Refs. [81–85]. We reserve their analysis to future work.

Performing integration over the dihadron angle in the following two ways:

$$\langle I_i\rangle_- \equiv \left[\int_0^{+1} d\cos\theta_\pi - \int_{-1}^{0} d\cos\theta_\pi\right] I_i,$$
$$\langle I_i\rangle_+ \equiv \int_{-1}^{+1} d\cos\theta_\pi I_i, \tag{54}$$

results in observables that depend only on the P-wave ($\langle I_i\rangle_+$ for $i=3$, 6, 9 and $\langle I_i\rangle_-$ for $i=4$, 5, 7, 8), receive noninterfering contributions from both the S- and the P-waves ($\langle I_i\rangle_+$ for $i=1$, 2), or depend on the interference of the two waves ($\langle I_i\rangle_-$ for $i=1$, 2 and $\langle I_i\rangle_+$ for $i=4$, 5, 7, 8). Explicitly,

$$\begin{aligned}\langle I_1\rangle_- &= \frac{1}{4}\mathrm{Re}\big(\mathcal{F}_S\mathcal{F}_P^*\big(\big(C_9^{\mathrm{eff}:S}+C_9^{\mathrm{NP}}-C_9'\big)\\ &\quad\times\big(C_9^{\mathrm{eff}:P}+C_9^{\mathrm{NP}}-C_9'\big)^*+|C_{10}-C_{10}'|^2\big)\big)\\ &\xrightarrow{\mathrm{SM}}\frac{1}{4}\mathrm{Re}\big(\mathcal{F}_S\mathcal{F}_P^*C_9^{\mathrm{eff}:S}\big(C_9^{\mathrm{eff}:P}\big)^*\big),\end{aligned} \tag{55}$$

$$\langle I_2\rangle_- = -\langle I_1\rangle_-, \tag{56}$$

$$\langle I_3\rangle_- = 0, \tag{57}$$

$$\frac{3}{2}\langle I_4\rangle_- = -\frac{1}{4}\mathrm{Re}(\mathcal{F}_P\mathcal{F}_\parallel^*)\rho_{1,P}^-\xrightarrow{\mathrm{SM}}-\frac{1}{4}\mathrm{Re}(\mathcal{F}_P\mathcal{F}_\parallel^*)|C_9^{\mathrm{eff}:P}|^2, \tag{58}$$

$$\frac{3}{2}\langle I_5\rangle_- = \left[\mathrm{Re}(\mathcal{F}_P\mathcal{F}_\perp^*)\mathrm{Re}\rho_2^+ + \mathrm{Im}(\mathcal{F}_P\mathcal{F}_\perp^*)\mathrm{Im}\rho_2^-\right]\xrightarrow{\mathrm{SM}}0, \tag{59}$$

$$\langle I_6\rangle_- = 0, \tag{60}$$

$$\frac{3}{2}\langle I_7\rangle_- = \mathrm{Im}(\mathcal{F}_P\mathcal{F}_\parallel^*)\delta\rho\xrightarrow{\mathrm{SM}}0, \tag{61}$$

$$\begin{aligned}\frac{3}{2}\langle I_8\rangle_- &= \frac{1}{2}\left[\mathrm{Re}(\mathcal{F}_P\mathcal{F}_\perp^*)\mathrm{Im}\rho_2^+ - \mathrm{Im}(\mathcal{F}_P\mathcal{F}_\perp^*)\mathrm{Re}\rho_2^-\right]\\ &\xrightarrow{\mathrm{SM}}-\frac{1}{4}\mathrm{Im}(\mathcal{F}_P\mathcal{F}_\perp^*)|C_9^{\mathrm{eff}:P}|^2,\end{aligned} \tag{62}$$

$$\langle I_9\rangle_- = 0, \tag{63}$$

and (note that $d^2\Gamma/dq^2dp^2 = 2\langle I_1\rangle_+ - \frac{2}{3}\langle I_2\rangle_+$)

$$\begin{aligned}\langle I_1\rangle_+ &= \frac{1}{8}\bigg[2|\mathcal{F}_S|^2\rho_{1,S}^- + \frac{2}{3}|\mathcal{F}_P|^2\rho_{1,P}^-\\ &\quad+2|\mathcal{F}_\parallel|^2\rho_{1,P}^- + 2|\mathcal{F}_\perp|^2\rho_{1,P}^+\bigg]\\ &\xrightarrow{\mathrm{SM}}+\frac{1}{8}\bigg\{2|\mathcal{F}_S|^2|C_9^{\mathrm{eff}:S}|^2\\ &\quad+\left[\frac{2}{3}|\mathcal{F}_P|^2+2(|\mathcal{F}_\parallel|^2+|\mathcal{F}_\perp|^2)\right]|C_9^{\mathrm{eff}:P}|^2\bigg\},\end{aligned} \tag{64}$$

$$\begin{aligned}\langle I_2\rangle_+ &= -\frac{1}{8}\bigg[2|\mathcal{F}_S|^2\rho_{1,S}^-\\ &\quad+\frac{2}{3}\{|\mathcal{F}_P|^2\rho_{1,P}^- - |\mathcal{F}_\parallel|^2\rho_{1,P}^- - |\mathcal{F}_\perp|^2\rho_{1,P}^+\}\bigg]\\ &\xrightarrow{\mathrm{SM}}-\frac{1}{8}\bigg\{2|\mathcal{F}_S|^2|C_9^{\mathrm{eff}:S}|^2\\ &\quad+\frac{2}{3}(|\mathcal{F}_P|^2-|\mathcal{F}_\parallel|^2-|\mathcal{F}_\perp|^2)|C_9^{\mathrm{eff}:P}|^2\bigg\},\end{aligned} \tag{65}$$

$$\begin{aligned}\langle I_3\rangle_+ &= \frac{1}{6}[|\mathcal{F}_\perp|^2\rho_{1,P}^+ - |\mathcal{F}_\parallel|^2\rho_{1,P}^-]\\ &\xrightarrow{\mathrm{SM}}\frac{1}{6}(|\mathcal{F}_\perp|^2-|\mathcal{F}_\parallel|^2)|C_9^{\mathrm{eff}:P}|^2,\end{aligned} \tag{66}$$

$$\begin{aligned}\frac{2}{\pi}\langle I_4\rangle_+ &= -\frac{1}{4}\mathrm{Re}\big[\mathcal{F}_S\mathcal{F}_\parallel^*((C_9^{\mathrm{eff}:S}+C_9^{\mathrm{NP}}-C_9')\\ &\quad\times(C_9^{\mathrm{eff}:P}+C_9^{\mathrm{NP}}-C_9')^*+|C_{10}-C_{10}'|^2)\big]\\ &\xrightarrow{\mathrm{SM}}-\frac{1}{4}\mathrm{Re}\big[\mathcal{F}_S\mathcal{F}_\parallel^*C_9^{\mathrm{eff}:S}(C_9^{\mathrm{eff}:P})^*\big],\end{aligned} \tag{67}$$

$$\begin{aligned}\frac{2}{\pi}\langle I_5\rangle_+ &= \frac{1}{2}\mathrm{Re}\big[\mathcal{F}_S\mathcal{F}_\perp^*((C_9^{\mathrm{eff}:S}+C_9^{\mathrm{NP}}-C_9')(C_{10}+C_{10}')^*\\ &\quad+(C_9^{\mathrm{eff}:P}+C_9^{\mathrm{NP}}+C_9')^*(C_{10}-C_{10}'))\big]\xrightarrow{\mathrm{SM}}0,\end{aligned} \tag{68}$$

$$\langle I_6\rangle_+ = -\frac{4}{3}\left[\mathrm{Re}(\mathcal{F}_\parallel\mathcal{F}_\perp^*)\mathrm{Re}\rho_2^+ + \mathrm{Im}(\mathcal{F}_\parallel\mathcal{F}_\perp^*)\mathrm{Im}\rho_2^-\right]\xrightarrow{\mathrm{SM}}0, \tag{69}$$

$$\begin{aligned}\frac{2}{\pi}\langle I_7\rangle_+ &= \frac{1}{2}\mathrm{Im}\big[\mathcal{F}_S\mathcal{F}_\parallel^*((C_9^{\mathrm{eff}:S}+C_9^{\mathrm{NP}}-C_9')\\ &\quad\times(C_{10}-C_{10}')^*+(C_9^{\mathrm{eff}:P}+C_9^{\mathrm{NP}}-C_9')^*\\ &\quad\times(C_{10}-C_{10}'))\big]\xrightarrow{\mathrm{SM}}0,\end{aligned} \tag{70}$$

$$\begin{aligned}\frac{2}{\pi}\langle I_8\rangle_+ = &-\frac{1}{4}\mathrm{Im}\big[\mathcal{F}_S\mathcal{F}_\perp^*\big((C_9^{\mathrm{eff}:S}+C_9^{\mathrm{NP}}-C_9')\\ &\times(C_9^{\mathrm{eff}:P}+C_9^{\mathrm{NP}}+C_9')^*\\ &+(C_{10}-C_{10}')(C_{10}+C_{10}')^*\big)\big]\\ &\xrightarrow{\mathrm{SM}} -\frac{1}{4}\mathrm{Im}\big[\mathcal{F}_S\mathcal{F}_\perp^* C_9^{\mathrm{eff}:S}(C_9^{\mathrm{eff}:P})^*\big],\end{aligned} \tag{71}$$

$$\begin{aligned}\langle I_9\rangle_+ = &\frac{2}{3}\big[\mathrm{Re}(\mathcal{F}_\perp\mathcal{F}_\parallel^*)\mathrm{Im}\rho_2^+ + \mathrm{Im}(\mathcal{F}_\perp\mathcal{F}_\parallel^*)\mathrm{Re}\rho_2^-\big]\\ &\xrightarrow{\mathrm{SM}} \frac{1}{3}\mathrm{Im}(\mathcal{F}_\perp\mathcal{F}_\parallel^*)|C_9^{\mathrm{eff}:P}|^2.\end{aligned} \tag{72}$$

We now define $\bar{I}_i$ as analogous of I_i for the CP-conjugated process. The new kinematical conventions are that θ_ℓ is the angle between the ℓ^--momentum and the $\bar{D}$-momentum in the dilepton center of mass frame, and θ_π is the angle between the π^+-momentum and the negative $\bar{D}$-momentum in the dipion center of mass frame, while, following the previous procedure to define the remaining angle ϕ', one has $\phi' = \pi - \phi$. In the comparison of the two processes certain angular observables acquire a sign under CP transformation due to kinematical considerations, $I_i \to \bar{I}_i$ for $i = 1, 2, 3, 4, 7$, while $I_j \to -\bar{I}_j$ for $j = 5, 6, 8, 9$. LHCb [2–4] provides measurements for the following CP-averaged S and CP-asymmetric A quantities: $\langle O_i\rangle = \langle I_i\rangle_{f(i)} \pm \langle \bar{I}_i\rangle_{f(i)}$ for $i = 1, 2, 3, 4, 7$, and $\langle O_j\rangle = \langle I_j\rangle_{f(j)} \mp \langle \bar{I}_j\rangle_{f(j)}$ for $j = 5, 6, 8, 9$, where $O \to S$ ($O \to A$) for the upper (respectively, lower) signs; these measurements by LHCb optimize the sensitivity to P-wave effects, namely, $f(i) = +$ for $i = 1, 2, 3, 6, 9$, while $f(j) = -$ for $j = 4, 5, 7, 8$ (see Table I). Since in the current work we neglect CP-odd contributions from the SM, the CP asymmetries of all angular observables vanish in the SM limit. The CP-averaged quantities are the following:

$$\begin{aligned}&\langle S_2\rangle(p^2,q^2) \equiv \langle I_2\rangle_+,\\ &\langle S_3\rangle(p^2,q^2) \equiv \langle I_3\rangle_+,\\ &\langle S_4\rangle(p^2,q^2) \equiv \langle I_4\rangle_-,\\ &\langle S_5\rangle(p^2,q^2) \equiv \langle I_5\rangle_- \xrightarrow{\mathrm{SM}} 0,\\ &\langle S_6\rangle(p^2,q^2) \equiv \langle I_6\rangle_+ \xrightarrow{\mathrm{SM}} 0,\\ &\langle S_7\rangle(p^2,q^2) \equiv \langle I_7\rangle_- \xrightarrow{\mathrm{SM}} 0,\\ &\langle S_8\rangle(p^2,q^2) \equiv \langle I_8\rangle_- \xrightarrow{\mathrm{SM}} \sim 0,\\ &\langle S_9\rangle(p^2,q^2) \equiv \langle I_9\rangle_+ \xrightarrow{\mathrm{SM}} \sim 0.\end{aligned} \tag{73}$$

The binned quantities quoted by Refs. [2–4] are defined as

$$\begin{aligned}&\langle O_k\rangle^{[q_{i_1}^2,q_{i_2}^2]} \equiv \frac{1}{\Gamma^{[q_{i_1}^2,q_{i_2}^2]}}\int \langle O_k\rangle^{[q_{i_1}^2,q_{i_2}^2]},\\ &O = S, A, \quad k = 1,\ldots,9,\end{aligned} \tag{74}$$

for a bin $[q_{i_1}^2, q_{i_2}^2]$, where the following shortcut notation has been employed:

$$\int f^{[q_{i_1}^2,q_{i_2}^2]} \equiv \int_{q_{i_1}^2}^{q_{i_2}^2} dq^2 \int_{p_{\mathrm{min}}^2}^{p_{\mathrm{max}}^2(q^2)} dp^2 f(p^2,q^2), \tag{75}$$

for any function f; the notation Γ^r designates the total width in the q^2-bin r. We stress that the observables $\langle S_8\rangle^r$ and $\langle S_9\rangle^r$, although vanishing in the SM when employing the approximation $C_9^{\mathrm{eff}:P}$ for any bin r due to our description of the phases encoded in the transversity form factors $\mathcal{F}_P$, $\mathcal{F}_\parallel$, and $\mathcal{F}_\perp$, obtain nonvanishing values in the original picture (i.e., before the introduction of effective C_9 coefficients). Nevertheless, these values remain very small, being suppressed due to the simple parametrizations of the $D \to \mathcal{R}$, $D \to \mathcal{V}$ form factors. Also note that from the above equations $\langle I_7\rangle_-$ seems to vanish even in the presence of NP. Although this is not the case when the original description is implemented (again, before the effective C_9 coefficients were introduced), the calculated values are still very suppressed for the same reason mentioned for $\langle S_8\rangle^r$ and $\langle S_9\rangle^r$. On the other hand, as discussed later its S-wave sensitive counterpart $\langle I_7\rangle_+$ yields values comparable to those of the other null-test observables for the same values of NP Wilson coefficients.

Some relations aiming to isolate the Wilson coefficients with potential phenomenological interest include (see also Ref. [18])

$$\begin{aligned}&\frac{\langle S_8\rangle(p^2,q^2)}{\langle A_5\rangle(p^2,q^2)} = \frac{1}{2}\frac{\mathrm{Im}\rho_2^+}{\mathrm{Re}\rho_2^+},\\ &\frac{\langle S_9\rangle(p^2,q^2)}{\langle A_6\rangle(p^2,q^2)} = -\frac{1}{2}\frac{\mathrm{Im}\rho_2^+}{\mathrm{Re}\rho_2^+},\\ &\frac{\langle S_5\rangle(p^2,q^2)}{\langle A_8\rangle(p^2,q^2)} = -2\frac{\mathrm{Im}\rho_2^-}{\mathrm{Re}\rho_2^-},\\ &\frac{\langle S_6\rangle(p^2,q^2)}{\langle A_9\rangle(p^2,q^2)} = 2\frac{\mathrm{Im}\rho_2^-}{\mathrm{Re}\rho_2^-},\end{aligned} \tag{76}$$

which are relevant only in the unbinned limit, since $C_9^{\mathrm{eff}:P}$ carries a dependence on kinematical variables.

IV. FITS AND PREDICTIONS

We search for footprints of the S-wave in three different types of observables. First (I), the ones related to the differential mass distributions, where the effect of the S- and P-waves is additive. Second (II), we examine the observables that probe the S- and P-wave interference. Third (III), we look into observables that vanish in the SM

TABLE I. Summary of the angular observables: the upper table contains $\langle\cdot\rangle_+$ quantities, while the lower one contains $\langle\cdot\rangle_-$ quantities. In the first column, a tick ✓ indicates an S-wave effect through its interference with the P-wave, an empty circle $\circ$ means that the S-wave manifests through an additive term to the P-wave instead of an interference term, and a cross ✗ indicates the absence of any S-wave effect. The SM dependencies on the effective Wilson coefficients (WCs) are given in the second column along with a typical value found for the integrated observables in the SM. The best fit values of the normalization and relative phases are considered for setting the numerical values given above. When two signs are shown, they correspond to different relative phases of the S- and P-waves (Δ_{SP} and $\Delta_{\rho\mathrm{NP}}$ are taken here to value 0 mod $\pi/2$). The integration range considered is $(0.78\ \mathrm{GeV})^2 < q^2(\ell^+\ell^-) < (1.1\ \mathrm{GeV})^2$. The third column indicates the dependence on the effective SM and on the NP WCs in the presence of a nonvanishing $\tilde{C}_{10} = V_{ub}V_{cb}^* C_{10}$, taken at its current upper bound, along with a typical value for the integrated observables. The Hermitian conjugate is also understood when the displayed combination of WCs is possibly complex.

$\int\langle I_i\rangle_+^r/\Gamma^r$		SM: $C_9^{\mathrm{NP}} = C_9' = C_{10} = C_{10}' = 0$		NP: $\tilde{C}_{10} = 0.43, C_9^{\mathrm{NP}} = C_9' = C_{10}' = 0$	
i	S-wave	WCs	Value [%]	WCs	Value [%]
1[a]	$\circ$	$\lvert C_9^{\mathrm{eff}:S}\rvert^2$, $\lvert C_9^{\mathrm{eff}:P}\rvert^2$	48	SM + $\lvert C_{10}\rvert^2$	48
2[a]	$\circ$	$\lvert C_9^{\mathrm{eff}:S}\rvert^2$, $\lvert C_9^{\mathrm{eff}:P}\rvert^2$	−7	SM + $\lvert C_{10}\rvert^2$	−7
3[a]	✗	$\lvert C_9^{\mathrm{eff}:P}\rvert^2$	−14	SM + $\lvert C_{10}\rvert^2$	−14
4	✓	$C_9^{\mathrm{eff}:S}(C_9^{\mathrm{eff}:P})^*$	±2	SM + $\lvert C_{10}\rvert^2$	±2
5	✓	$\cdots$	0	$C_9^{\mathrm{eff}:S}C_{10}^* + C_{10}(C_9^{\mathrm{eff}:P})^*$	±0.1
6[a]	✗	$\cdots$	0	$\mathrm{Re}[C_9^{\mathrm{eff}:P}C_{10}^*]$	±0.3
7	✓	$\cdots$	0	$C_9^{\mathrm{eff}:S}C_{10}^* + C_{10}(C_9^{\mathrm{eff}:P})^*$	±0.4
8	✓	$C_9^{\mathrm{eff}:S}(C_9^{\mathrm{eff}:P})^*$	±1	SM + $\lvert C_{10}\rvert^2$	±1
9[a]	✗	$\lvert C_9^{\mathrm{eff}:P}\rvert^2$	~0	SM + $\lvert C_{10}\rvert^2$	~0

$\int\langle I_i\rangle_-^r/\Gamma^r$		SM: $C_9^{\mathrm{NP}} = C_9' = C_{10} = C_{10}' = 0$		NP: $\tilde{C}_{10} = 0.43, C_9^{\mathrm{NP}} = C_9' = C_{10}' = 0$	
i	S-wave	WCs	Value [%]	WCs	Value [%]
1	✓	$C_9^{\mathrm{eff}:S}(C_9^{\mathrm{eff}:P})^*$	∓2	SM + $\lvert C_{10}\rvert^2$	∓2
2	✓	$C_9^{\mathrm{eff}:S}(C_9^{\mathrm{eff}:P})^*$	±2	SM + $\lvert C_{10}\rvert^2$	±2
4[a]	✗	$\lvert C_9^{\mathrm{eff}:P}\rvert^2$	20	SM + $\lvert C_{10}\rvert^2$	20
5[a]	✗	$\cdots$	0	$\mathrm{Re}[C_9^{\mathrm{eff}:P}C_{10}^*]$	±0.2
7[a]	✗	$\cdots$	0	$\mathrm{Re}[C_9^{\mathrm{eff}:P}C_{10}^*]$	~0
8[a]	✗	$\lvert C_9^{\mathrm{eff}:P}\rvert^2$	~0	SM + $\lvert C_{10}\rvert^2$	~0

[a]These cases indicate quantities already measured by LHCb [2–4].

and find some that are sensitive to NP only in the presence of the S-wave; we compare these to observables that are sensitive to NP only in the presence of the P-wave. Cases (I) and (II) are discussed in Sec. IV A; we will in particular extract in this section parameters accounting for normalizations, namely, $\{a_\omega, a_S(0)/A_1(0), A_1(0)B_{\rho^0}, B_\phi/B_{\rho^0}, B_\omega^{(S)}/B_{\rho^0}^{(S)}, B_\phi^{(S)}/B_{\rho^0}^{(S)}\}$, and relative strong phases among intermediate resonances, namely, ϕ_ω and Δ_i, $i = 1, 3, 4$. Because of the suppression factor ϵ_ω, we do not include B_ω nor Δ_2 in this list. The ratio $B_{\rho^0}^{(S)}/B_{\rho^0}$ is set to the unit, and $a_S(0)$ is adjusted to determine the overall contribution of the S-wave. It is implicitly assumed that NP contamination is negligible in the differential mass distributions. Case (III) is the subject of Sec. IV B. The three types of observables (I)–(III) are easily identified in Table I; the values of the most interesting observables over distinct q^2 bins will be discussed in detail in the following, and are given in Tables II–IV that deal with cases (I)–(III), respectively. We stress that we also make comparisons to the LHCb dataset that optimizes the sensitivity to the P-wave. We have not included theory uncertainties (e.g., stemming from the use of the factorization approach) in the following discussion beyond the ones attached to the unknown parameters we have fitted for.

A. SM fits and predictions

The large statistics and fine binning of Refs. [2–4] allow for a precision numerical study. The global fit we perform combines bins of both differential mass distributions as functions of the invariant mass of the lepton (q^2) or pion (p^2) pairs. We note that no correlations among bins of $d\Gamma/dp^2$ and $d\Gamma/dq^2$ have been made available in those

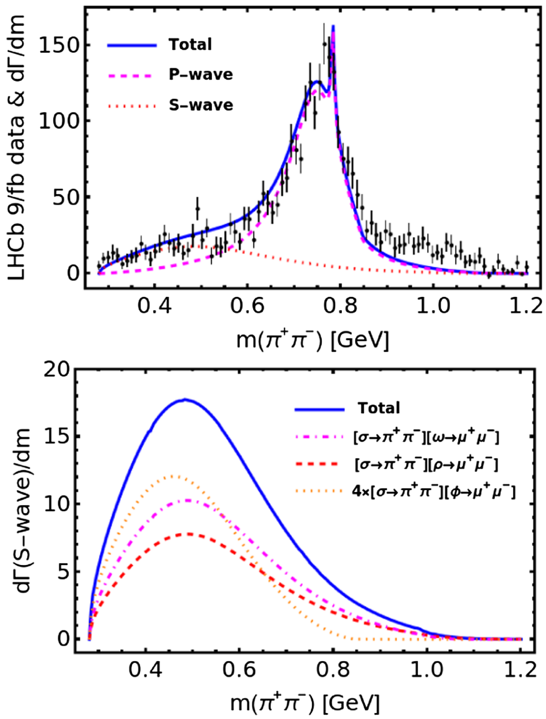

FIG. 3. The prediction for the differential decay rate $d\Gamma/dm$ and LHCb data over the dihadron invariant mass $m(\pi^+\pi^-) \equiv \sqrt{p^2}$ [2–4]. Top: the contributions from the S-wave (dotted red curve) and the P-wave (dashed magenta curve) add up to the full resonant contribution (solid blue curve). Bottom: components of the S-wave contribution: $\sigma\rho^0$ (dashed red curve), $\sigma\omega$ (dot-dashed magenta curve), and $\sigma\phi$ (dotted orange curve, multiplied by 4 for an easier comparison).

references.[11] We first discuss the features of the $d\Gamma/dp^2$ distribution, which is crucial to establish the σ contribution. Being a very broad resonance, the effect of including the σ might be difficult to spot. However, we do observe a clear contribution in the differential decay rate as a function of p^2; see Fig. 3. It is clearly seen by eye that including σ in the theoretical prediction improves the quality of the fit; quantitatively, $\chi^2_{\mathrm{min;w/o}\,\sigma} - \chi^2_{\mathrm{min}} = 10^2$, clearly favoring its inclusion.[12] The $d\Gamma/dp^2$ distribution is also used to probe the small $\omega \to \pi^+\pi^-$ contribution, together with its relative phase with respect to the ρ^0 contribution. There is good evidence of the presence of such ω: $\chi^2_{\mathrm{min;w/o}\,\omega} - \chi^2_{\mathrm{min}} = 4^2$, which is also approximately distributed as a χ^2 with a single degree of freedom. In performing the fits, we have excluded the region ± 70 MeV around the mass of the K^0_S to account for the possibility of contamination from $K^0_S \to \pi^+\pi^-$.[13] Also, we have considered data points up to 0.9 GeV, since beyond this energy virtual kaon pairs (i.e., below their actual threshold)[14] along with other resonances such as $f_0(980)$ start manifesting more strongly (in the former case, in the dispersive part of the amplitude). The presence of other resonances that include beyond the S- and P-waves also the D-wave, together with the isospin-two and bremsstrahlung contributions, are likely to be at the origin of the poor comparison between our prediction and the data in the high-p^2 region (see the top panel of Fig. 3). The value of $\chi^2_{\mathrm{min}}/N_{\mathrm{d.o.f.}} \simeq 2$ (where $N_{\mathrm{d.o.f.}} \simeq 77$) has been found, driven mainly by the $d\Gamma/dp^2$ dataset.

We now discuss the features of the $d\Gamma/dq^2$ distribution. We fit the data of Refs. [2–4] in the region $q^2 \geq m^2_\rho$, in order to avoid the many other resonances that we do not address in the present work, shown in Fig. 1. Figure 4 displays the result of our fit, which achieves a good qualitative description of the data. Quantitatively, the fit does not perform well at the ϕ resonance, underestimating the branching ratio therein; the fit indicates that a broader width of the ϕ should be considered; i.e., the predicted values closer to m_ϕ tend to be overestimated, while peripheral values away from m_ϕ by $\Gamma^0_\phi = 4.25$ MeV [28] tend to be underestimated. Accordingly, we observe that a much better fit of the $d\Gamma/dq^2$ data is achieved when increasing the width of the ϕ by about 60%; namely, the χ^2_{min} drops significantly. This effect should be due to limited momentum resolution at LHCb (bin migration is found to be negligible in Ref. [5]), whose effect has not been "unfolded," thus broadening the ϕ peak; efficiency variations, instead, are taken into account [86]. We fix the ϕ width to Γ^0_ϕ in our theoretical predictions, and to circumvent the later resolution issue we collect the four bins around the ϕ peak into a single bin; this is the situation depicted in Fig. 4.

From the global fit we find the following value for the overall normalization factor (intervals of about 3σ C.L. are provided in this section):

$$0.8 \lesssim A_1(0) B_{\rho^0} \lesssim 1.2, \tag{77}$$

for the extraction of which we employ also information about the total branching fraction provided in Eq. (1). A value of $A_1(0)$ close to 0.6 as in Ref. [88] implies B_{ρ^0} of

[11] There is, of course, a correlation between $\int dp^2 d\Gamma/dp^2$ and $\int dq^2 d\Gamma/dq^2$ accounting for the total partial width that we do not include in our fit.

[12] For this test only, we have reintroduced back to the fit B_ω and Δ_2, so the improvement comes mainly from the $d\Gamma/dp^2$ distribution.

[13] This procedure is adopted from Ref. [29], which, however, is a different experiment (and process). In the case of LHCb, K^0_S contributions are not explicitly vetoed. However, vertexing eliminates to a certain degree the aforementioned K^0_S contamination, but there is no quantitative estimate of the resulting efficiency [86].

[14] Note that this is a source of violation of the Zweig rule; see, e.g., Ref. [87].

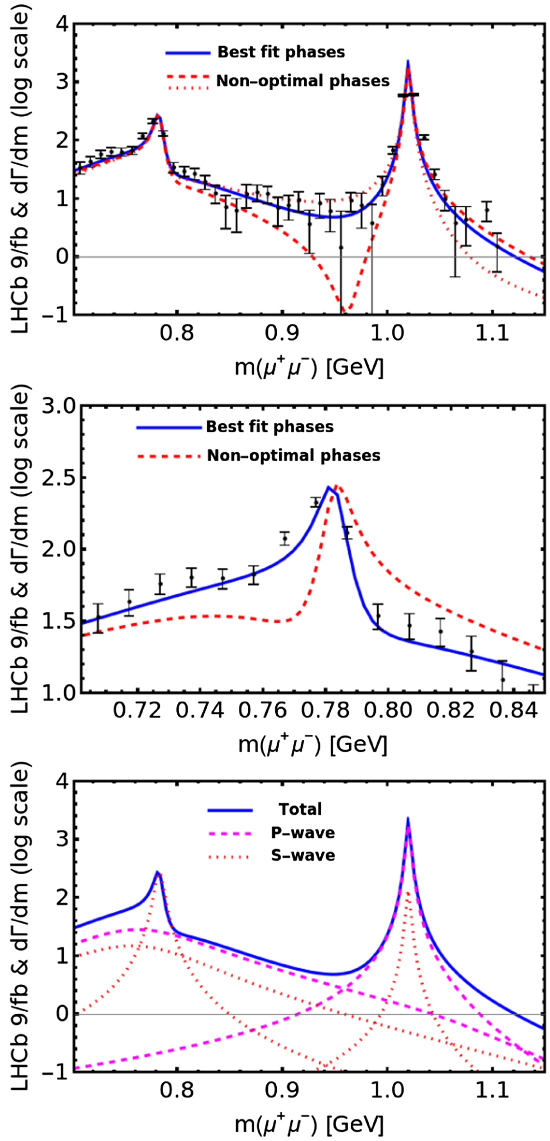

FIG. 4. The differential decay rate $d\Gamma/dm$ (in blue) and LHCb data over the dilepton invariant mass $m(\mu^+\mu^-) \equiv \sqrt{q^2}$ [2–4]. Top: the dashed (dotted) red curve displaying nonoptimal phases corresponds to the optimal Δ_1 added with $\pi/2$ $(-3\pi/4)$. Middle: the dashed red curve displaying nonoptimal phases corresponds to the optimal Δ_4 added with $5\pi/4$. Bottom: P- and S-wave components, in dashed magenta and dotted red, respectively; interference terms are set to zero.

around 1.8. For ratios of normalization factors (or "fudge factors") we have

$$0.8 \lesssim B_\phi/B_{\rho^0} \lesssim 0.9, \tag{78}$$

$$0.9 \lesssim B_\omega^{(S)}/B_{\rho^0}^{(S)} \lesssim 1.1, \tag{79}$$

$$0.05 \lesssim B_\phi^{(S)}/B_{\rho^0}^{(S)} \lesssim 0.27. \tag{80}$$

The $D^0 \to \pi^+\pi^-[\phi, \omega \to \mu^+\mu^-]$ resonant branching ratios constrain precisely the parameters B_ϕ/B_{ρ^0} and $B_\omega^{(S)}/B_{\rho^0}^{(S)}$. The $D^0 \to [\rho^0 \to \pi^+\pi^-][\phi \to \mu^+\mu^-]$ is the largely dominant P-wave contribution. The inclusion of $d\Gamma/dp^2$ data has an important impact in limiting the size of $B_\phi^{(S)}/B_{\rho^0}^{(S)}$, which reflects differently compared to the other two contributions $\sigma\omega$ and $\sigma\rho^0$; see the bottom panel of Fig. 3, due to the different available p^2 intervals as seen from Fig. 1. It is evident that an important deviation from naive factorization shows up in the extraction of $B_\phi^{(S)}/B_{\rho^0}^{(S)}$, which lies substantially away from 1.[15] It is interesting to point out that the contribution from $\sigma\phi$ also turns out to be suppressed in the amplitude analysis of $D^0 \to K^+K^-\pi^+\pi^-$ by LHCb [35]. We also extract

$$0.001 \lesssim a_\omega \lesssim 0.005, \tag{81}$$

$$1.1\pi \lesssim \phi_\omega \lesssim 1.7\pi, \tag{82}$$

$$39 \text{ GeV} \lesssim \frac{a_S(0)}{A_1(0)} \lesssim 62 \text{ GeV}, \tag{83}$$

which compare relatively well with $a_\omega \simeq 0.006$, $\phi_\omega \simeq 0.9\pi$, and $a_S(0)/A_1(0) \simeq 24$ GeV for the analogous semileptonic decay $D^+ \to \pi^+\pi^-e^+\nu_e$ [29]; see Appendix B for further discussion.

The fit is also used to extract the following range for the relative angle $\Delta_1 = \delta_{\{\rho^0/\omega,\rho^0\}} - \delta_{\{\rho^0/\omega,\phi\}}$ (see the top panel of Fig. 4):

$$0.5\pi \lesssim \Delta_1 \lesssim 0.9\pi, \tag{84}$$

while $\Delta_3 = \delta_{\{\sigma,\rho^0\}} - \delta_{\{\sigma,\phi\}}$ remains unconstrained, since the contribution from the σ plays a less important role in the region between the ρ^0 and ϕ resonances with respect to the P-wave contribution. As it is clear from the top panel of Fig. 4, this strong phase has a huge impact in the latter inter-resonant region and the very-high energy region above the ϕ resonance, implying modulations of the predicted branching ratios by orders of magnitude in both cases. It is interesting to point out the possible correlation between the inter-resonant and the very-high energy regions due to the ϕ line shape, e.g., a large suppression of the SM prediction in the very-high energy region (making then this region more sensitive to NP contributions), can be correlated to a relatively large branching ratio in the inter-resonant region; a similar effect is seen in Ref. [17]. In the middle panel of Fig. 4, we illustrate the dependence of our prediction on the remaining strong-phase differences. As it has been discussed around Eq. (32),

[15] A sizable deviation from factorization is seen in the context of $B \to K\mu^+\mu^-$ decays; see, e.g., Ref. [77].

TABLE II. SM predictions for the nonvanishing observables which only receive P-wave contributions ($\int\langle I_3\rangle_+^r$, $\int\langle I_4\rangle_-^r$), and where the effect of the S-wave is additive (i.e., $\Gamma^r = \Gamma^r_{\rho^0/\omega} + \Gamma^r_\sigma$ and $\int\langle I_2\rangle_+^r = \int\langle I_2\rangle^r_{+,\rho^0/\omega} + \int\langle I_2\rangle^r_{+,\sigma}$); a subscript σ indicates that only the S-wave is kept. The relation $\Gamma^r = 2(\int\langle I_1\rangle_+^r - \int\langle I_2\rangle_+^r/3)$ holds true. For comparison with LHCb [2–4], $\langle S_2\rangle^r = \int\langle I_2\rangle_+^r/\Gamma^r$, $\langle S_3\rangle^r = \int\langle I_3\rangle_+^r/\Gamma^r$, and $\langle S_4\rangle^r = \int\langle I_4\rangle_-^r/\Gamma^r$; as mentioned at the beginning of Sec. III, $\langle S_4\rangle^r = -\langle S_4\rangle^r|_{\mathrm{LHCb}}$. Relevant definitions can be found in Sec. III; see in particular Eqs. (74) and (75). The decay rate and the I_i's both need to be multiplied by a common constant factor, $|C_2\lambda_d e G_F/\sqrt{2}|^2 \frac{e^2}{m_D}\times 10^{-4} = 2.4\times 10^{-19}$, with G_F, m_D, and Γ^r in GeV.

q^2-bin r	Γ^r (SM)	$\frac{\Gamma^r_\sigma}{\Gamma^r}$ [%]	$\int\langle I_2\rangle_+^r \times 100$	$\frac{\int\langle I_2\rangle^r_{+,\sigma}}{\int\langle I_2\rangle^r_+}$ [%]	$\int\langle I_3\rangle_+^r \times 100$	$\int\langle I_4\rangle_-^r \times 100$
$r^{(\rho:\,\mathrm{sup})}$	[0.64, 0.87]	[23, 43]	[−16, −8.5]	[59, 78]	[−7.2, −4.7]	[8.3, 13]
$r^{(\phi:\,\mathrm{inf})}$	[1.6, 1.9]	[0.3, 8]	[−11, −6.2]	[3, 45]	[−30, −26]	[36, 41]
$r^{(\phi:\,\mathrm{sup})}$	[1.2, 1.3]	[0.8, 10]	[−8.7, −4.3]	[8, 53]	[−22, −19]	[26, 29]

the contribution of the $\omega \to \ell^+\ell^-$ paired with the pion pair in a P-wave is suppressed;[16] on the other hand, the $\omega \to \ell^+\ell^-$ can manifest when combined with the pion pair in the S-wave; see the bottom panel of Fig. 4. We then find for $\Delta_4 = \delta_{\{\sigma,\rho^0\}} - \delta_{\{\sigma,\omega\}}$:

$$0.2\pi \lesssim \Delta_4 \lesssim 0.5\pi. \tag{85}$$

It is rather difficult to provide interpretations to the extracted ranges of values for Δ_1 and Δ_4, or make comparisons to other processes; note that the ρ^0 and the ω or the ϕ are in different isospin irreducible representations, so that the dynamics involved in the rescattering processes with the second resonance (the ρ^0/ω in the case of Δ_1, and the σ in the case of Δ_4) is expected to be substantially different.

We now discuss our predictions and the available data for the angular observables. Following LHCb [2–4], we define the ranges:

$$\begin{aligned} r^{(\rho:\,\mathrm{sup})} &\equiv [0.78^2, 0.95^2]\ \mathrm{GeV}^2,\\ r^{(\phi:\,\mathrm{inf})} &\equiv [0.95^2, 1.02^2]\ \mathrm{GeV}^2,\\ r^{(\phi:\,\mathrm{sup})} &\equiv [1.02^2, 1.1^2]\ \mathrm{GeV}^2. \end{aligned} \tag{86}$$

Since we focus on the high-energy window of Fig. 1, we will discuss predictions for these three bins, while LHCb also provides results for the bins $[0.212^2, 0.525^2]$ GeV^2 and $[0.565^2, 0.78^2]$ GeV^2; the bin $[0.565^2, 0.78^2]$ GeV^2, however, is also used for determining the total branching ratio distribution as a function of p^2 (the branching ratio outside these four q^2-bins is highly suppressed). In Table II we present predicted values for those observables that do not vanish in the SM, in particular in the presence of the S-wave, in cases where it does not interfere with the P-wave. As seen in this table, the σ provides significant contributions, as large as 10%–40% in the binned branching ratios. This fraction is even larger in the case of $\int\langle I_2\rangle^r_{+,\sigma}$, which contributes to the binned branching ratio $\Gamma^r = 2(\int\langle I_1\rangle_+^r - \int\langle I_2\rangle_+^r/3)$, reaching up to about 50%–80% of $\int\langle I_2\rangle_+^r$. The dominance of the S-wave in this observable can be attributed to a suppression of the P-wave contribution, due to a cancellation among the transversity form factors as seen from Eq. (65) (also manifesting in the case of $\int\langle I_3\rangle_+^r$), which, on the other hand, are added constructively in the case of $\langle I_1\rangle_+^r$ [cf. Eq. (64)]. In performing a comparison of our predictions to LHCb data of the observables $\langle S_2\rangle^r$, $\langle S_3\rangle^r$, and $\langle S_4\rangle^r$ in the three bins $r^{(\rho:\,\mathrm{sup})}$, $r^{(\phi:\,\mathrm{inf})}$, and $r^{(\phi:\,\mathrm{sup})}$ we obtain a p-value of $\mathcal{O}(10)\%$.

As we have seen, our predictions for the angular observables $\langle S_7\rangle^r$, $\langle S_8\rangle^r$, and $\langle S_9\rangle^r$ (approximately) vanish, even in the presence of NP; we find, however, a poor comparison with the hypothesis that they are all zero in the five bins of Eq. (86), $\chi^2/N_{\mathrm{d.o.f.}} \simeq 2.4$ (where $N_{\mathrm{d.o.f.}} \simeq 15$), or a p-value of 0.2%, due to $\langle S_9\rangle^r$. This may indicate a missing description of the relative strong phases among the transversity form factors $\mathcal{F}_P$, $\mathcal{F}_\parallel$, and $\mathcal{F}_\perp$. [Including in this latter test the $\langle S_5\rangle^r$ and $\langle S_6\rangle^r$ observables, which also vanish in the SM, we get $\chi^2/N_{\mathrm{d.o.f.}} \simeq 2.0$ (where $N_{\mathrm{d.o.f.}} \simeq 25$), or a p-value of 0.2%, which is small also as a consequence of including $\langle S_9\rangle^r$.] The violation of CP is surely exciting in the context of charm physics, where a sizable level of CP violation has been recently measured by LHCb [89,90] in hadronic two-body charm-meson decays; see Ref. [91] for a theoretical discussion. On the other hand, the CP asymmetries in rare charm-meson decays are consistent with zero, since in this case we find that p-value $= 84\%$. Note that statistical correlations among bins and across observables are provided by the LHCb analysis; they are small, but have been included. Systematic uncertainties are smaller than statistical uncertainties and are fully correlated (we use the techniques discussed in Ref. [92] to combine both categories of uncertainties in the presence of correlations).

In Table III we provide the values for nonvanishing angular observables that probe the interference of the

[16] We note that allowing for large effects much beyond naive factorization, namely, $B_\omega \gg B_{\rho^0}$, allows for a good fit of the $d\Gamma/dq^2$ data even in the absence of the S-wave.

TABLE III. SM predictions for the nonvanishing angular observables that probe the interference between the S- and P-waves. The parameters appearing stand for $c_{SP} \equiv \cos(\Delta_{SP})$ and $s_{SP} \equiv \sin(\Delta_{SP})$. The relation $\int \langle I_1 \rangle_-^r = -\int \langle I_2 \rangle_-^r$ holds true. Relevant definitions can be found in Sec. III; see in particular Eqs. (74) and (75). The same overall multiplicative factor shown in the caption of Table II applies.

q^2-bin r	$\int \langle I_2 \rangle_-^r \times 100$
$r^{(\rho:\,\mathrm{sup})}$	$[-6.6,-0.8]c_{SP}+[-2.3,-1.1]s_{SP}$
$r^{(\phi:\,\mathrm{inf})}$	$[-7.7,6.1]c_{SP}+[-5.3,8.2]s_{SP}$
$r^{(\phi:\,\mathrm{sup})}$	$[-7.1,3.0]c_{SP}+[-5.0,5.4]s_{SP}$

q^2-bin r	$\int \langle I_4 \rangle_+^r \times 100$
$r^{(\rho:\,\mathrm{sup})}$	$[0.8,5.9]c_{SP}+[0.4,1.6]s_{SP}$
$r^{(\phi:\,\mathrm{inf})}$	$[-6.7,8.3]c_{SP}+[-8.6,5.4]s_{SP}$
$r^{(\phi:\,\mathrm{sup})}$	$[-3.1,7.6]c_{SP}+[-5.9,5.5]s_{SP}$

q^2-bin r	$\int \langle I_8 \rangle_+^r \times 100$
$r^{(\rho:\,\mathrm{sup})}$	$[-3.0,-0.2]c_{SP}+[-0.4,0.4]s_{SP}$
$r^{(\phi:\,\mathrm{inf})}$	$[-4.6,4.5]c_{SP}+[-3.4,4.0]s_{SP}$
$r^{(\phi:\,\mathrm{sup})}$	$[-2.6,3.3]c_{SP}+[-1.7,3.3]s_{SP}$

S- and P-waves. These observables depend on the relative phase $\Delta_{SP} = \delta_{\{\sigma,\rho^0\}} - \delta_{\{\rho^0/\omega,\rho^0\}}$ between the S- and P-waves. None of the experimentally provided observables from Refs. [2–4] is sensitive to this phase; hence, it is left as a free parameter. A future experimental analysis would probe this phase difference, possibly in combination with the differential distribution over the dihadron angle, as discussed in the next paragraph. As seen in the table, some sizable values are found, typically smaller but of similar order compared to the ones provided in Table II that are insensitive to the S-wave.

Finally, as announced in the Introduction, the S-wave can produce distinguished signatures in the differential branching ratio as a function of the angular variables describing the topology of the rare decay. To illustrate this point, consider

$$\frac{d\Gamma}{d\cos\theta_\pi} = \langle I_1 \rangle^r_{+,\rho^0/\omega} + \langle I_2 \rangle^r_{+,\rho^0/\omega}(1-4\cos^2\theta_\pi) - \frac{4}{3}\langle I_2 \rangle^r_{+,\sigma} - \frac{8}{3}\langle I_2 \rangle^r_- \cos\theta_\pi, \quad (87)$$

after integration over the q^2-bin r, where the contributions from the S- and P-waves alone are indicated in subscript (here, the σ and ρ^0/ω resonances, respectively), and the last term in the right-hand side (i.e., the last term in the second line) probes their interference. As seen in Fig. 5, the presence of the S-wave can produce an asymmetry of the distribution with respect to $\cos\theta_\pi = 0$. This provides motivation for binned measurements of the branching ratio as a function of the angular variables.

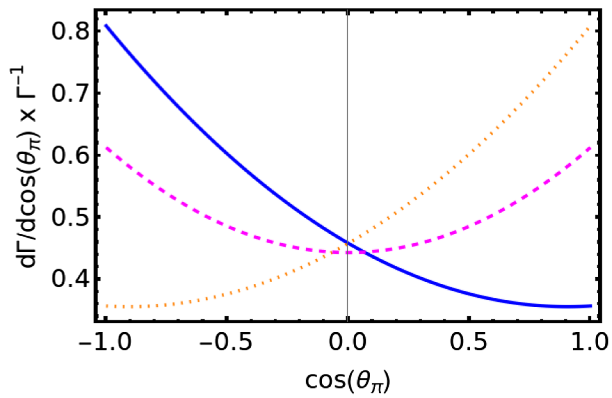

FIG. 5. The differential decay rate, after integration of dilepton energies over the range $r^{(\rho:\,\mathrm{sup})} \cup r^{(\phi:\,\mathrm{inf})} \cup r^{(\phi:\,\mathrm{sup})} = [0.78^2, 1.1^2]$ GeV^2, as a function of $\cos(\theta_\pi)$. In dashed magenta the observable is shown in the absence of the S-wave contribution [rescaled such that $\int_{-1}^{1} d\cos(\theta_\pi) d\Gamma/d\cos(\theta_\pi)/\Gamma = 1$]. The solid blue and dotted orange lines correspond to extreme cases reached for certain values of the phase difference Δ_{SP} between the S- and P-waves that maximize their interference. As it is clear from the figure, the interference of the S- and P-waves can generate a distinguished asymmetry.

B. Semileptonic operators from generic NP

We want to know the impact of having dimension-six operators that can mediate the transition $c \to u\ell^+\ell^-$ at the quark level due to interactions mediated by heavy NP. We focus on vector and axial-vector structures. Present bounds at 95% C.L. are [22]

$$|\tilde{C}_9^{\mathrm{NP}}|, |\tilde{C}_9'| < 1.2, \qquad |\tilde{C}_{10}^{(\prime)}| < 0.43, \quad (88)$$

where $|\tilde{C}| = |V_{ub}V_{cb}^* C|$ and the former bound results from the $D^+ \to \pi^+\mu^+\mu^-$ branching ratio [93], while the second results from the $D^0 \to \mu^+\mu^-$ branching ratio [94]. Slightly better bounds are found from collider searches for contact interactions manifesting in $pp \to \mu^+\mu^-$ [95]. In view of these constraints, it is justified to assume that in the kinematical ranges analyzed NP does not affect the previous discussion about the differential branching ratio as a function of the invariant masses of pion and lepton pairs. However, NP could still affect the differential branching ratio in the low and very-high dilepton invariant mass regions [17]. It can also affect distinct angular observables as we now discuss.

As seen from the expressions provided in Sec. III, there are distinct observables that depend on these Wilson coefficients. In Table IV we provide predictions for those observables sensitive to the SM-NP interference in the presence of a nonvanishing C_{10} Wilson coefficient [its SM value is very suppressed, as discussed around Eq. (2)]. The cases $\langle I_5 \rangle_-$ and $\langle I_6 \rangle_+$ are sensitive to the SM-NP interference through the P-wave, while $\langle I_7 \rangle_-$ approximately vanishes. These observables, which isolate the

TABLE IV. Observables that vanish in the SM, arising from the interference of the P-wave and NP, here calculated for $C_9' = C_{10}' = C_9^{\mathrm{NP}} = 0$ and nonzero C_{10}. The parameters appearing stand for $c_{\rho\mathrm{NP}} = \cos(\Delta_{\rho\mathrm{NP}})$ and $s_{\rho\mathrm{NP}} = \sin(\Delta_{\rho\mathrm{NP}})$. The other P-wave dependent observable $\langle I_7\rangle_-$ approximately vanishes. The NP does not interfere with the SM in the decay rate and can thus be neglected. Relevant definitions can be found in Sec. III [see in particular Eqs. (74) and (75)]. The same overall multiplicative factor shown in the caption of Table II applies; additionally, there is an extra $\tilde{C}_{10}$ that multiplies the observables.

q^2-bin r	$\int\langle I_5\rangle_-^r \times 100$
$r^{(\rho:\,\mathrm{sup})}$	$[0.49, 0.83]c_{\rho\mathrm{NP}} + [-1.5, -1.3]s_{\rho\mathrm{NP}}$
$r^{(\phi:\,\mathrm{inf})}$	$[-0.36, 0.50]c_{\rho\mathrm{NP}} + [-0.83, -0.60]s_{\rho\mathrm{NP}}$
$r^{(\phi:\,\mathrm{sup})}$	$[0.31, 0.66]c_{\rho\mathrm{NP}} + [-0.09, 0.49]s_{\rho\mathrm{NP}}$
q^2-bin r	$\int\langle I_6\rangle_+^r \times 100$
$r^{(\rho:\,\mathrm{sup})}$	$[0.7, 1.2]c_{\rho\mathrm{NP}} + [-2.1, -1.7]s_{\rho\mathrm{NP}}$
$r^{(\phi:\,\mathrm{inf})}$	$[-0.57, 0.78]c_{\rho\mathrm{NP}} + [-1.3, -1.0]s_{\rho\mathrm{NP}}$
$r^{(\phi:\,\mathrm{sup})}$	$[0.5, 1.1]c_{\rho\mathrm{NP}} + [-0.14, 0.78]s_{\rho\mathrm{NP}}$

NP interference with the SM P-wave, are given as functions of the phase difference

$$\Delta_{\rho\mathrm{NP}} \equiv \delta_{\{\rho^0/\omega,\rho^0\}} - \delta_{Q_{10}}, \tag{89}$$

where $\delta_{Q_{10}}$ allows for a possible strong phase when considering insertions of the Q_{10} operator (beyond the one from the pion pair line shape). Predictions are shown in Table IV.

On the other hand, the cases $\langle I_5\rangle_+$ and $\langle I_7\rangle_+$ are sensitive to the SM-NP interference in the presence of the S-wave. These observables depend on the above phase $\Delta_{\rho\mathrm{NP}}$ together with Δ_{SP}. The latter phase difference can be probed based on the observables whose predictions are given in Table III and the observable shown in Fig. 5. Given the dependence on both phase differences, we do not give explicitly the expressions for the related angular observables. By varying these phases, we stress that we find values of the angular observables comparable to the ones found for the analogous P-wave null tests in Table IV.

Given the bounds shown in Eq. (88), detecting NP requires subpercentage precision in the measurement of the angular observables. Having reached such precision, some bins of the angular observables sensitive to the S-wave provide additional complementary information to favor or disfavor an observation of a possible NP manifestation based on the P-wave cases. In the future, a global fit could extract all relevant phases, together with possible NP contributions. It is possible that a clever strategy could circumvent the need to extract at least some of the strong phases affecting the angular observables.

V. CONCLUSIONS

Recent experimental data by LHCb open up the opportunity for precision physics with rare charm-meson decays, a task that can be assisted by complementary information coming from experiments such as BESIII, and by Belle II in different rare decay modes. For this reason, better theoretical predictions are needed, in particular the description of resonances, without which it will not be possible to disentangle non-SM contributions from the large SM background; better theoretical predictions of the SM are also needed in order to describe possible interference terms with non-SM contributions. We employ a factorization model for the inclusion of intermediate hadronic states contributing to $D^0 \to \pi^+\pi^-\ell^+\ell^-$ in the SM and discuss in detail different contributing topologies. Within this framework, the novelty of this work concerns the inclusion of the lightest scalar isoscalar state, which is a very broad resonance manifesting in long-distance pion pair interactions and impacts a large portion of the allowed phase space; see Fig. 1. We highlight that $D^0 \to \pi^+\pi^-\ell^+\ell^-$ data already show the clear emergence of such S-wave effects; see Fig. 3. Moreover, current data also allow the study of the strong phases among intermediate resonances; see Fig. 4.

The decay $D^0 \to \pi^+\pi^-\ell^+\ell^-$ offers the possibility to define a rich set of angular observables. We then discuss angular observables that are sensitive to both the S- and P-waves. Predictions are given in Tables II and III. We have been able to understand the overall pattern of the measured angular observables $\langle S_i\rangle^r$, $i = 2, \ldots, 8$, testing P-wave contributions in distinct q^2-bins r. To further improve our understanding of SM contributions, we suggest experimentalists measure additional observables to further test and better characterize the contributions of the S-wave, such as following the strategy illustrated in Fig. 5.

Such additional observables also have an interest other than improving nonperturbative aspects of the SM description. Indeed, the search for NP constitutes one of the main motivations for looking into this category of rare decay processes. If any deviation is seen while performing a null test of the SM, a comprehensive analysis will be needed to verify and characterize it. We emphasize the potential for complementary tests of NP via its interference with the SM in the presence of the S-wave, which provide distinct null tests of the SM, as seen from Table IV.

To improve the description of the differential branching ratio, in particular the one as a function of the pion pair invariant mass, future theoretical directions include incorporating other S- and P-wave resonances and the D-wave following a similar theoretical framework, isospin-two contributions, and the addition of cascade decays. More studies will be needed to understand the set of angular observables measured by LHCb in more detail, since with our simple factorization model some tension appears in the description of the angular observable $\langle S_9 \rangle^r$. It would also be interesting to extend our analysis to include $D^0 \to K^+K^-\mu^+\mu^-$ and radiative decay modes.

ACKNOWLEDGMENTS

We thank Fernando Abudinén, Damir Becirevic, Thomas Blake, Luka Leskovec, Lei Li, Serena Maccolini, Dominik Mitzel, Juan Nieves, Eulogio Oset, Tommaso Pajero, Antonio Pich, Luka Santelj, and Shulei Zhang for helpful communication. E. S. is grateful to Gudrun Hiller and the rest of the participants for helpful discussions during the "First CharmInDor mini workshop." This work has been supported by MCIN/AEI/10.13039/501100011033, Grants No. PID2020–114473GB-I00 and No. PRE2018-085325, and by Generalitat Valenciana, Grant No. PROMETEO/2021/071. This project has received funding from the European Union's Horizon 2020 research and innovation program under the Marie Sklodowska-Curie Grant Agreement No. 101031558. S. F. acknowledges the financial support from the Slovenian Research Agency (research core funding No. P1-0035). L. V. S. is grateful for the hospitality of the Jožef Stefan Institute and the CERN-TH group where part of this research was executed.

APPENDIX A: HADRONIC INPUTS

1. Decay constants

We have from Ref. [76]

$$\begin{aligned} \langle \phi | \bar{s}\gamma_\mu s | 0 \rangle &= \epsilon^*_\mu m_\phi f_\phi, \\ \hat{c}^q_\omega \langle \omega | \bar{q}\gamma_\mu q | 0 \rangle &= \epsilon^*_\mu m_\omega f^{(q)}_\omega, \\ \hat{c}^q_{\rho^0} \langle \rho^0 | \bar{q}\gamma_\mu q | 0 \rangle &= \epsilon^*_\mu m_{\rho^0} f^{(q)}_{\rho^0}, \end{aligned} \tag{A1}$$

with $\hat{c}^u_{\rho^0} = -\hat{c}^d_{\rho^0} = \hat{c}^u_\omega = \hat{c}^d_\omega = \sqrt{2}$. We consider a single decay constant for both matrix elements of u- and d-quark bilinears, i.e., $f^{(q)}_\omega \to f_\omega$ and $f^{(q)}_{\rho^0} \to f_{\rho^0}$, which is good enough for our purposes. The decay constants are then

$$\begin{aligned} f_{\rho^0} &= 216(3)\ \text{MeV}, \\ f_\omega &= 197(8)\ \text{MeV}, \\ f_\phi &= 233(4)\ \text{MeV}. \end{aligned} \tag{A2}$$

(Mixing effects, of ω with ρ^0 and ω with ϕ, have been included, but are small.)

2. Form factors

For the $D \to \mathcal{V}$ form factors, for both $\mathcal{V} = \rho^0, \omega$, we use the nearest pole approximation introduced in Ref. [75], which has the general form

$$F(q^2) = F(0) / \left(1 - \frac{q^2}{m^2_{\text{pole}}}\right). \tag{A3}$$

The pole masses implemented are 2.42 GeV ($J^P = 1^+$) for $F = A_1$ and A_2, and 2.01 GeV ($J^P = 1^-$) for $F = V$. We define

$$r_V = \frac{V(0)}{A_1(0)}, \qquad r_2 = \frac{A_2(0)}{A_1(0)}, \tag{A4}$$

for which Ref. [29] gives $r_V = 1.695 \pm 0.083 \pm 0.051$ and $r_2 = 0.845 \pm 0.056 \pm 0.039$ (with a correlation of $\rho_{r_V, r_2} = -0.206$), where the first (second) uncertainty is statistical (respectively, systematic).

3. Line shapes

We reproduce the line shape of $f_0(500)$ [26]:

$$\mathcal{A}_S(s) = \frac{1}{M^2 - s - g_1^2(s) \frac{s - s_A}{M^2 - s_A} z(s) - iM\Gamma_{\text{tot}}(s)}, \tag{A5}$$

$$\Gamma_{\text{tot}}(s) = \sum_{i=1}^{4} \Gamma_i(s), \tag{A6}$$

$$M\Gamma_1(s) = g_1^2(s) \frac{s - s_A}{M^2 - s_A} \rho_1(s), \tag{A7}$$

$$\rho_1(s) = \sqrt{1 - 4m_\pi^2/s}, \tag{A8}$$

$$g_1^2(s) = M(b_1 + b_2 s) \exp[-(s - M^2)/A], \tag{A9}$$

$$z(s) = j_1(s) - j_1(M^2), \tag{A10}$$

$$j_1(s) = \frac{1}{\pi}\left[2 + \rho_1(s) \log\left(\frac{1 - \rho_1(s)}{1 + \rho_1(s)}\right)\right], \tag{A11}$$

$$\begin{aligned} M\Gamma_2(s) = 0.6 g_1^2(s)(s/M^2) \exp[&-\alpha(s - 4\,m_K^2)\Theta(s - 4\,m_K^2) \\ &-\alpha'(4\,m_K^2 - s)\Theta(4\,m_K^2 - s)]\rho_2(s), \end{aligned} \tag{A12}$$

$$\begin{aligned} \rho_2(s) = &\sqrt{1 - 4m_K^2/s}\Theta(s - 4\,m_K^2) \\ &+ i\sqrt{4\,m_K^2/s - 1}\Theta(4\,m_K^2 - s), \end{aligned} \tag{A13}$$

$$\begin{aligned} M\Gamma_3(s) = 0.2 g_1^2(s)(s/M^2) \exp[&-\alpha(s - 4\,m_\eta^2)\Theta(s - 4\,m_\eta^2) \\ &-\alpha'(4\,m_\eta^2 - s)\Theta(4\,m_\eta^2 - s)]\rho_3(s), \end{aligned} \tag{A14}$$

$$\begin{aligned} \rho_3(s) = &\sqrt{1 - 4\,m_\eta^2/s}\Theta(s - 4\,m_\eta^2) \\ &+ i\sqrt{4\,m_\eta^2/s - 1}\Theta(4\,m_\eta^2 - s), \end{aligned} \tag{A15}$$

$$M\Gamma_4(s) = M g_{4\pi} \rho_{4\pi}(s)/\rho_{4\pi}(M^2)\Theta(s - 16\,m_\pi^2), \tag{A16}$$

$$\rho_{4\pi}(s) = 1.0/[1 + \exp(7.082 - 2.845\ s/\mathrm{GeV}^2)], \qquad (A17)$$

$$s_A \simeq 0.41\, m_\pi^2, \qquad \alpha = 1.3\ \mathrm{GeV}^{-2}, \qquad \alpha' = 2.1\ \mathrm{GeV}^{-2}, \qquad (A18)$$

and [solution (iii) of Ref. [26]] $M = 0.953$ GeV, $b_1 = 1.302$ GeV, $b_2 = 0.340/\mathrm{GeV}$, $A = 2.426\ \mathrm{GeV}^2$, $g_{4\pi} = 0.011$ GeV.

For the line shape of the $\rho(770)^0$ in $\pi^+\pi^-$ decays, we adopt the Gounaris-Sakurai parametrization [78]:

$$P_{\rho^0}(s) = m_{\rho^0}^2 - s + f(s) - i m_{\rho^0}\Gamma_{\rho^0}(s), \qquad (A19)$$

$$f(s) = \Gamma_{\rho^0}^0 \frac{m_{\rho^0}^2}{k_{\rho^0}^3}\{k(s)^2[h(s) - h(m_{\rho^0}^2)] + k_{\rho^0}^2(m_{\rho^0}^2 - s)h'(m_{\rho^0}^2)\}, \qquad (A20)$$

$$\Gamma_{\rho^0}(s) = \Gamma_{\rho^0}^0 \left(\frac{k(s)}{k_{\rho^0}}\right)^3 \frac{m_{\rho^0}}{\sqrt{s}}, \qquad (A21)$$

$$h(s) = \frac{2}{\pi}\frac{k(s)}{\sqrt{s}}\log\left(\frac{\sqrt{s} + 2k(s)}{2m_\pi}\right), \qquad (A22)$$

$$k(s) = \left(\frac{1}{4}s - m_\pi^2\right)^{1/2}, \qquad k_{\rho^0} = \left(\frac{1}{4}m_{\rho^0}^2 - m_\pi^2\right)^{1/2}. \qquad (A23)$$

We also have [29,96,97]

$$\mathrm{RBW}_\omega(s) = \frac{s}{m_\omega^2 - s - i m_\omega \Gamma_\omega^0}, \qquad (A24)$$

and

$$F_{\mathrm{BW}}(p^2) = B(p^*)/B(p_0^*), \qquad (A25)$$

$$B(p^*) = \frac{1}{\sqrt{1 + r_{\mathrm{BW}}^2 (p^*)^2}}. \qquad (A26)$$

The value of r_{BW} is taken to be 3.0/GeV (i.e., the inverse of a nonperturbative scale) [29]. The function $p^*(p^2) = \sqrt{\lambda(p^2, m_\pi^2, m_\pi^2)}/(2\sqrt{p^2})$, and $p_0^* = p^*(m_{\rho^0}^2)$. The ϕ and the ω line shapes, when the latter decays to the lepton pair, are just Breit-Wigner line shapes:

$$P_\phi(s) = m_\phi^2 - s - i m_\phi \Gamma_\phi^0, \qquad P_\omega(s) = m_\omega^2 - s - i m_\omega \Gamma_\omega^0, \qquad (A27)$$

The masses and widths are [28]

$$m_{\rho^0} = 775.3\ \mathrm{MeV}, \qquad \Gamma_{\rho^0}^0 = 147.4\ \mathrm{MeV}, \qquad (A28)$$

$$m_\omega = 782.7\ \mathrm{MeV}, \qquad \Gamma_\omega^0 = 8.7\ \mathrm{MeV}, \qquad (A29)$$

$$m_\phi = 1019.46\ \mathrm{MeV}, \qquad \Gamma_\phi^0 = 4.25\ \mathrm{MeV}. \qquad (A30)$$

APPENDIX B: FURTHER COMMENTS ON SEMILEPTONIC DECAYS

To reproduce the values in Table I of Ref. [29] relative to D^+ decays, we find $a_S(0) = 8.6 \pm 0.4$ GeV, $a_\omega = 0.006 \pm 0.001$, and $A_1(0) = 0.36$. The strong phases extracted in their analysis are $\phi_S = 3.4044 \pm 0.0738$, which is somewhat analogous of Δ_{SP} defined in the main text, and $\phi_\omega = 2.93 \pm 0.17$ [97]; this latter angle is consistent with π from the isospin decomposition of the $(\bar{d}d)_V$ current that generates the states ρ^0 and ω. Instead, we employ in this work the values extracted from a fit to the data of Refs. [2–4]; see Fig. 3. In doing so, we obtain the values quoted in Eq. (81), which in the case of $a_S(0)/A_1(0)$ is about 2 times larger than the value shown above. The comparison, however, is not straightforward, since the σ contributes in three dynamical ways when combined with the ρ^0, ω, ϕ that lead to the lepton pair. Note that the resonance that decays into pion pairs originates from both u- (in the W-type topology) and d-quark pairs (in the J-type topology), which differs from the situation depicted above for ϕ_ω. Likely, the extraction of the phase ϕ_ω from data is contaminated by the presence of further resonances discussed in the main text that we do not include in our analysis, and the presence of further intermediate hadrons (i.e., vector mesons that lead to the lepton pair) in the full charm-meson decay process.

(For comparison with Ref. [30], there is an overall normalization factor, adapted for the line shape in use here:

$$\alpha_{GS} = \sqrt{\frac{3\pi\mathcal{B}_{\rho^0}}{p_0^*\Gamma_{\rho^0}^0}\frac{\Gamma_{\rho^0}^0}{m_{\rho^0}}}, \qquad \mathcal{B}_{\rho^0} = 1.) \qquad (B1)$$

[1] S. L. Glashow, J. Iliopoulos, and L. Maiani, Weak interactions with lepton-hadron symmetry, Phys. Rev. D **2**, 1285 (1970).
[2] Roel Aaij *et al.*, Angular analysis of $D^0 \to \pi^+\pi^-\mu^+\mu^-$ and $D^0 \to K^+K^-\mu^+\mu^-$ decays and search for CP violation, Phys. Rev. Lett. **128**, 221801 (2022).
[3] https://journals.aps.org/prl/supplemental/10.1103/PhysRevLett.128.221801/LHCb-PAPER-2021-035-supplemental.pdf (LHCb Supplemental Material).
[4] https://lhcbproject.web.cern.ch/Publications/LHCbProjectPublic/LHCb-PAPER-2021-035.html (LHCb Supplemental Material).
[5] R Aaij *et al.*, Search for the decay $D_0 \to \pi^+\pi^-\mu^+\mu^-$, Phys. Lett. B **728**, 234 (2014).
[6] Roel Aaij *et al.*, Observation of D^0 meson decays to $\pi^+\pi^-\mu^+\mu^-$ and $K^+K^-\mu^+\mu^-$ final states, Phys. Rev. Lett. **119**, 181805 (2017).
[7] Roel Aaij *et al.*, Measurement of angular and CP asymmetries in $D^0 \to \pi^+\pi^-\mu^+\mu^-$ and $D^0 \to K^+K^-\mu^+\mu^-$ decays, Phys. Rev. Lett. **121**, 091801 (2018).
[8] https://lhcbproject.web.cern.ch/Publications/LHCbProjectPublic/LHCb-PAPER-2018-020.html (LHCb Supplemental Material). Note in particular relative efficiencies in $D^0 \to \pi^+\pi^-\mu^+\mu^-$ as a function of $\sin 2\phi$, $\cos\theta_\ell$, $\cos\theta_\pi$, $m(\mu^+\mu^-)$, and $m(\pi^+\pi^-)$; the latter is high for the low-$m(\pi^+\pi^-)$ region.
[9] A. Freyberger *et al.*, Limits on flavor changing neutral currents in D^0 meson decays, Phys. Rev. Lett. **76**, 3065 (1996); Phys. Rev. Lett. **77**, 2147(E) (1996).
[10] M. Ablikim *et al.*, Search for the rare decays $D \to h(h')e^+e^-$, Phys. Rev. D **97**, 072015 (2018).
[11] M. Achasov *et al.*, STCF conceptual design report (Volume 1): Physics & detector, Front. Phys. (Beijing) **19**, 14701 (2024).
[12] S. Fajfer, Sasa Prelovsek, and P. Singer, Resonant and nonresonant contributions to the weak $D \to Vl^+l^-$ decays, Phys. Rev. D **58**, 094038 (1998).
[13] Gustavo Burdman, Eugene Golowich, JoAnne L. Hewett, and Sandip Pakvasa, Rare charm decays in the Standard Model and beyond, Phys. Rev. D **66**, 014009 (2002).
[14] Svjetlana Fajfer and Sasa Prelovsek, Effects of littlest Higgs model in rare D meson decays, Phys. Rev. D **73**, 054026 (2006).
[15] Ikaros I. Bigi and Ayan Paul, On CP asymmetries in two-, three- and four-body D decays, J. High Energy Phys. 03 (2012) 021.
[16] Luigi Cappiello, Oscar Cata, and Giancarlo D'Ambrosio, Standard Model prediction and new physics tests for $D^0 \to h^+h^-\ell^+\ell^-(h = \pi, K : \ell = e, \mu)$, J. High Energy Phys. 04 (2013) 135.
[17] Stefan De Boer and Gudrun Hiller, Null tests from angular distributions in $D \to P_1P_2l^+l^-$, $l = e, \mu$ decays on and off peak, Phys. Rev. D **98**, 035041 (2018).
[18] Thorsten Feldmann, Bastian Müller, and Dirk Seidel, $D \to \rho\ell^+\ell^-$ decays in the QCD factorization approach, J. High Energy Phys. 08 (2017) 105.
[19] Aoife Bharucha, Diogo Boito, and Cédric Méaux, Disentangling QCD and new physics in $D^+ \to \pi^+\ell^+\ell^-$, J. High Energy Phys. 04 (2021) 158.
[20] Ayan Paul, Ikaros I. Bigi, and Stefan Recksiegel, On $D \to X_u l^+l^-$ within the Standard Model and frameworks like the littlest Higgs model with T parity, Phys. Rev. D **83**, 114006 (2011).
[21] Stefan de Boer and Gudrun Hiller, Flavor and new physics opportunities with rare charm decays into leptons, Phys. Rev. D **93**, 074001 (2016).
[22] Svjetlana Fajfer and Nejc Košnik, Prospects of discovering new physics in rare charm decays, Eur. Phys. J. C **75**, 567 (2015).
[23] Rigo Bause, Marcel Golz, Gudrun Hiller, and Andrey Tayduganov, The new physics reach of null tests with $D \to \pi\ell\ell$ and $D_s \to K\ell\ell$ decays, Eur. Phys. J. C **80**, 65 (2020); Eur. Phys. J. C **81**, 219(E) (2021).
[24] Marxil Sánchez, Genaro Toledo, and I. Heredia De La Cruz, Taming the long distance effects in the $D_s^+ \to \pi^+\ell^-\ell^+$ decay, Phys. Rev. D **106**, 073002 (2022).
[25] Hector Gisbert, Marcel Golz, and Dominik Stefan Mitzel, Theoretical and experimental status of rare charm decays, Mod. Phys. Lett. A **36**, 2130002 (2021).
[26] D. V. Bugg, The mass of the sigma pole, J. Phys. G **34**, 151 (2007).
[27] J. R. Pelaez, From controversy to precision on the sigma meson: A review on the status of the non-ordinary $f_0(500)$ resonance, Phys. Rep. **658**, 1 (2016).
[28] R. L. Workman *et al.*, Review of particle physics, Prog. Theor. Exp. Phys. **2022**, 083C01 (2022).
[29] Medina Ablikim *et al.*, Observation of $D^+ \to f_0(500)e^+\nu_e$ and improved measurements of $D \to \rho e^+\nu_e$, Phys. Rev. Lett. **122**, 062001 (2019).
[30] P. del Amo Sanchez *et al.*, Analysis of the $D^+ \to K^-\pi^+e^+\nu_e$ decay channel, Phys. Rev. D **83**, 072001 (2011).
[31] J. M. Link *et al.*, Evidence for new interference phenomena in the decay $D^+ \to K^-\pi^+\mu^+\nu$, Phys. Lett. B **535**, 43 (2002).
[32] R. A. Briere *et al.*, Analysis of $D^+ \to K^-\pi^+e^+\nu_e$ and $D^+ \to K^-\pi^+\mu^+\nu_\mu$ semileptonic decays, Phys. Rev. D **81**, 112001 (2010).
[33] Philippe d'Argent, Nicola Skidmore, Jack Benton, Jeremy Dalseno, Evelina Gersabeck, Sam Harnew, Paras Naik, Claire Prouve, and Jonas Rademacker, Amplitude analyses of $D^0 \to \pi^+\pi^-\pi^+\pi^-$ and $D^0 \to K^+K^-\pi^+\pi^-$ decays, J. High Energy Phys. 05 (2017) 143.
[34] Medina Ablikim *et al.*, Amplitude analysis of $D^0 \to \pi^+\pi^-\pi^+\pi^-$ and $\pi^+\pi^-\pi^0\pi^0$, arXiv:2312.02524.
[35] Roel Aaij *et al.*, Search for CP violation through an amplitude analysis of $D^0 \to K^+K^-\pi^+\pi^-$ decays, J. High Energy Phys. 02 (2019) 126.
[36] F. E. Low, Bremsstrahlung of very low-energy quanta in elementary particle collisions, Phys. Rev. **110**, 974 (1958).
[37] N. B. Durusoy, M. Baubillier, R. George, M. Goldberg, A. M. Touchard, N. Armenise, M. T. Fogli Muciaccia, and A. Silvestri, Study of the $I = 2\pi\pi$ scattering from the reaction $\pi^-d \to \pi^-\pi^- \quad p_s p$ at 9.0 GeV/c, Phys. Lett. **45B**, 517 (1973).
[38] R. Garcia-Martin, R. Kaminski, J. R. Pelaez, and J. Ruiz de Elvira, Precise determination of the $f_0(600)$ and $f_0(980)$ pole parameters from a dispersive data analysis, Phys. Rev. Lett. **107**, 072001 (2011).
[39] Jose Ramon Pelaez, Arkaitz Rodas, and Jacobo Ruiz de Elvira, $f_0(1370)$ controversy from dispersive meson-meson

scattering data analyses, Phys. Rev. Lett. **130**, 051902 (2023).

[40] L. M. Sehgal and M. Wanninger, *CP* violation in the decay $K_L \to \pi^+\pi^-e^+e^-$, Phys. Rev. D **46**, 1035 (1992); Phys. Rev. D **46**, 5209(E) (1992).

[41] John K. Elwood, Mark B. Wise, and Martin J. Savage, $K_L \to \pi^+\pi^-e^+e^-$, Phys. Rev. D **52**, 5095 (1995); Phys. Rev. D **53**, 2855(E) (1996).

[42] Hannes Pichl, $K \to \pi\pi e^+e^-$ decays and chiral low-energy constants, Eur. Phys. J. C **20**, 371 (2001).

[43] Vincenzo Cirigliano, Gerhard Ecker, Helmut Neufeld, Antonio Pich, and Jorge Portoles, Kaon decays in the standard model, Rev. Mod. Phys. **84**, 399 (2012).

[44] L. Cappiello, O. Cata, G. D'Ambrosio, and Dao-Neng Gao, $K^+ \to pi^+ pi^0 e^+ e^-$: A novel short-distance probe, Eur. Phys. J. C **72**, 1872 (2012); Eur. Phys. J. C **72**, 2208(E) (2012).

[45] J. Bijnens, G. Colangelo, G. Ecker, and J. Gasser, Semileptonic kaon decays, arXiv:hep-ph/9411311.

[46] Damir Becirevic and Andrey Tayduganov, Impact of $B \to K_0^*\ell^+\ell^-$ on the new physics search in $B \to K^*\ell^+\ell^-$ decay, Nucl. Phys. **B868**, 368 (2013).

[47] Thomas Blake, Ulrik Egede, and Alex Shires, The effect of S-wave interference on the $B^0 \to K^{*0}\ell^+\ell^-$ angular observables, J. High Energy Phys. 03 (2013) 027.

[48] Christoph Bobeth, Gudrun Hiller, and Danny van Dyk, General analysis of $\bar{B} \to \bar{K}^{(*)}\ell^+\ell^-$ decays at low recoil, Phys. Rev. D **87**, 034016 (2013).

[49] Michael Döring, Ulf-G. Meißner, and Wei Wang, Chiral dynamics and S-wave contributions in semileptonic B decays, J. High Energy Phys. 10 (2013) 011.

[50] Diganta Das, Gudrun Hiller, Martin Jung, and Alex Shires, The $\bar{B} \to \bar{K}\pi\ell\ell$ and $\bar{B}_s \to \bar{K}K\ell\ell$ distributions at low hadronic recoil, J. High Energy Phys. 09 (2014) 109.

[51] Marcel Algueró, Paula Alvarez Cartelle, Alexander Mclean Marshall, Pere Masjuan, Joaquim Matias, Michael Andrew McCann, Mitesh Patel, Konstantinos A. Petridis, and Mark Smith, A complete description of P- and S-wave contributions to the $B^0 \to K^+\pi^-\ell^+\ell^-$ decay, J. High Energy Phys. 12 (2021) 085.

[52] Sébastien Descotes-Genon, Alexander Khodjamirian, Javier Virto, and K. Keri Vos, Light-cone sum rules for S-wave $B \to K\pi$ form factors, J. High Energy Phys. 06 (2023) 034.

[53] Roel Aaij *et al.*, Measurements of the S-wave fraction in $B^0 \to K^+\pi^-\mu^+\mu^-$ decays and the $B^0 \to K^*(892)^0\mu^+\mu^-$ differential branching fraction, J. High Energy Phys. 11 (2016) 047; J. High Energy Phys. 04 (2017) 142(E).

[54] Roel Aaij *et al.*, Differential branching fraction and angular moments analysis of the decay $B^0 \to K^+\pi^-\mu^+\mu^-$ in the $K^*_{0,2}(1430)^0$ region, J. High Energy Phys. 12 (2016) 065.

[55] W. H. Liang and E. Oset, B^0 and B_s^0 decays into $J/\psi f_0(980)$ and $J/\psi f_0(500)$ and the nature of the scalar resonances, Phys. Lett. B **737**, 70 (2014).

[56] J. T. Daub, C. Hanhart, and B. Kubis, A model-independent analysis of final-state interactions in $\bar{B}^0_{d/s} \to J/\psi\pi\pi$, J. High Energy Phys. 02 (2016) 009.

[57] Stefan Ropertz, Christoph Hanhart, and Bastian Kubis, A new parametrization for the scalar pion form factors, Eur. Phys. J. C **78**, 1000 (2018).

[58] Roel Aaij *et al.*, Measurement of the resonant and *CP* components in $\bar{B}^0 \to J/\psi\pi^+\pi^-$ decays, Phys. Rev. D **90**, 012003 (2014).

[59] Bernard Aubert *et al.*, Branching fraction and charge asymmetry measurements in $B \to J/\psi\pi\pi$ decays, Phys. Rev. D **76**, 031101 (2007).

[60] Roel Aaij *et al.*, Precise measurement of the f_s/f_d ratio of fragmentation fractions and of B_s^0 decay branching fractions, Phys. Rev. D **104**, 032005 (2021).

[61] J. Li *et al.*, Observation of $B_s^0 \to J/\psi f_0(980)$ and evidence for $B_s^0 \to J/\psi f_0(1370)$, Phys. Rev. Lett. **106**, 121802 (2011).

[62] Xian-Wei Kang, Bastian Kubis, Christoph Hanhart, and Ulf-G. Meißner, B_{l4} decays and the extraction of $|V_{ub}|$, Phys. Rev. D **89**, 053015 (2014).

[63] Sven Faller, Thorsten Feldmann, Alexander Khodjamirian, Thomas Mannel, and Danny van Dyk, Disentangling the decay observables in $B^- \to \pi^+\pi^-\ell^-\bar{\nu}_\ell$, Phys. Rev. D **89**, 014015 (2014).

[64] Luka Leskovec, Stefan Meinel, Marcus Petschlies, John Negele, Srijit Paul, Andrew Pochinsky, and Gumaro Rendon, A lattice QCD study of the $B \to \pi\pi\ell\bar{\nu}$ transition, Proc. Sci. LATTICE2022 (**2023**) 416.

[65] Damir Becirevic, Svjetlana Fajfer, Ivan Nisandzic, and Andrey Tayduganov, Angular distributions of $\bar{B} \to D^{(*)}\ell\bar{\nu}_\ell$ decays and search of new physics, Nucl. Phys. **B946**, 114707 (2019).

[66] Alain Le Yaouanc, Jean-Pierre Leroy, and Patrick Roudeau, Model for nonleptonic and semileptonic decays by $\bar{B}^0 \to D^{**}$ transitions with $\mathrm{BR}(j=1/2) \ll \mathrm{BR}(j=3/2)$ using the Leibovich-Ligeti-Stewart-Wise schem, Phys. Rev. D **105**, 013004 (2022).

[67] Nico Gubernari, Alexander Khodjamirian, Rusa Mandal, and Thomas Mannel, $B \to D_0^*$ and $B_s \to D_{s0}^*$ form factors from QCD light-cone sum rules, J. High Energy Phys. 12 (2023) 015.

[68] Erik J. Gustafson, Florian Herren, Ruth S. Van de Water, Raynette van Tonder, and Michael L. Wagman, A model independent description of $B \to D\pi\ell\nu$ decays, arXiv:2311.00864.

[69] Gerhard Buchalla, Andrzej J. Buras, and Markus E. Lautenbacher, Weak decays beyond leading logarithms, Rev. Mod. Phys. **68**, 1125 (1996).

[70] Stefan de Boer, Bastian Müller, and Dirk Seidel, Higher-order Wilson coefficients for $c \to u$ transitions in the standard model, J. High Energy Phys. 08 (2016) 091.

[71] Rigo Bause, Hector Gisbert, Marcel Golz, and Gudrun Hiller, Rare charm $\mathbf{c} \to \mathbf{u}\boldsymbol{\nu}\bar{\boldsymbol{\nu}}$ dineutrino null tests for e^+e^- machines, Phys. Rev. D **103**, 015033 (2021).

[72] Ling-Yun Dai and Michael R. Pennington, Comprehensive amplitude analysis of $\gamma\gamma \to \pi^+\pi^-, \pi^0\pi^0$ and $\bar{K}K$ below 1.5 GeV, Phys. Rev. D **90**, 036004 (2014).

[73] Antonio Pich, Effective field theory with Nambu-Goldstone modes, arXiv:1804.05664.

[74] Manfred Bauer, B. Stech, and M. Wirbel, Exclusive nonleptonic decays of $D-$, D_s-, and B mesons, Z. Phys. C **34**, 103 (1987).

[75] M. Wirbel, B. Stech, and Manfred Bauer, Exclusive semileptonic decays of heavy mesons, Z. Phys. C **29**, 637 (1985).

[76] Aoife Bharucha, David M. Straub, and Roman Zwicky, $B \to V\ell^+\ell^-$ in the standard model from light-cone sum rules, J. High Energy Phys. 08 (2016) 098.
[77] James Lyon and Roman Zwicky, Resonances gone topsy turvy—The charm of QCD or new physics in $b \to s\ell^+\ell^-$?, arXiv:1406.0566,
[78] G. J. Gounaris and J. J. Sakurai, Finite width corrections to the vector meson dominance prediction for $\rho \to e^+e^-$, Phys. Rev. Lett. **21**, 244 (1968).
[79] Clarence L. Y. Lee, Ming Lu, and Mark B. Wise, B_{l4} and D_{l4} decay, Phys. Rev. D **46**, 5040 (1992).
[80] Alexander Khodjamirian, *Hadron Form Factors: From Basic Phenomenology to QCD Sum Rules* (CRC Press, Taylor & Francis Group, Boca Raton, FL, USA, 2020).
[81] Gustavo Burdman, Eugene Golowich, JoAnne L. Hewett, and Sandip Pakvasa, Radiative weak decays of charm mesons, Phys. Rev. D **52**, 6383 (1995).
[82] Christoph Greub, Tobias Hurth, Mikolaj Misiak, and Daniel Wyler, The $c \to u\gamma$ contribution to weak radiative charm decay, Phys. Lett. B **382**, 415 (1996).
[83] Svjetlana Fajfer, Anita Prapotnik, and Paul Singer, Cabibbo allowed $D \to K\pi\gamma$ decays, Phys. Rev. D **66**, 074002 (2002).
[84] Nico Adolph, Joachim Brod, and Gudrun Hiller, Radiative three-body D-meson decays in and beyond the standard model, Eur. Phys. J. C **81**, 45 (2021).
[85] Nico Adolph and Gudrun Hiller, Probing QCD dynamics and the standard model with $D^+_{(s)} \to P_1^+ P_2^0 \gamma$ decays, J. High Energy Phys. 06 (2021) 155.
[86] Dominik Mitzel (private communication).
[87] John F. Donoghue, J. Gasser, and H. Leutwyler, The decay of a light Higgs boson, Nucl. Phys. **B343**, 341 (1990).
[88] D. Melikhov and B. Stech, Weak form-factors for heavy meson decays: An update, Phys. Rev. D **62**, 014006 (2000).
[89] Roel Aaij *et al.*, Observation of CP violation in charm decays, Phys. Rev. Lett. **122**, 211803 (2019).
[90] R. Aaij *et al.*, Measurement of the time-integrated CP asymmetry in $D^0 \to K^-K^+$ decays, Phys. Rev. Lett. **131**, 091802 (2023).
[91] Antonio Pich, Eleftheria Solomonidi, and Luiz Vale Silva, Final-state interactions in the CP asymmetries of charm-meson two-body decays, Phys. Rev. D **108**, 036026 (2023).
[92] Jérôme Charles, Sébastien Descotes-Genon, Valentin Niess, and Luiz Vale Silva, Modeling theoretical uncertainties in phenomenological analyses for particle physics, Eur. Phys. J. C **77**, 214 (2017).
[93] Roel Aaij *et al.*, Searches for 25 rare and forbidden decays of D^+ and D_s^+ mesons, J. High Energy Phys. 06 (2021) 044.
[94] R. Aaij *et al.*, Search for rare decays of D^0 mesons into two muons, Phys. Rev. Lett. **131**, 041804 (2023).
[95] Javier Fuentes-Martin, Admir Greljo, Jorge Martin Camalich, and José David Ruiz-Alvarez, Charm physics confronts high-p$_T$ lepton tails, J. High Energy Phys. 11 (2020) 080.
[96] R. R. Akhmetshin *et al.*, Measurement of $e^+e^- \to \pi^+\pi^-$ cross-section with CMD-2 around ρ meson, Phys. Lett. B **527**, 161 (2002).
[97] Shulei Zhang (private communication).